

Article

Monitoring of Lithium Contents in Lithium Ores and Concentrate-Assessment Using X-ray Diffraction (XRD)

Herbert Pöllmann ^{1,*} and Uwe König ²

¹ Department of Mineralogy, Institute of Geosciences and Geography, Martin-Luther Halle-Wittenberg University, 06108 Halle, Germany

² Malvern Panalytical B.V., 7602 EA Almelo, The Netherlands; uwe.konig@panalytical.com

* Correspondence: herbert.poellmann@geo.uni-halle.de

Abstract: Lithium plays an increasing role in battery applications, but is also used in ceramics and other chemical applications. Therefore, a higher demand can be expected for the coming years. Lithium occurs in nature mainly in different mineralizations but also in large salt lakes in dry areas. As lithium cannot normally be analyzed using XRF-techniques (XRF = X-ray Fluorescence), the element must be analyzed by time consuming wet chemical treatment techniques. This paper concentrates on XRD techniques for the quantitative analysis of lithium minerals and the resulting recalculation using additional statistical methods of the lithium contents. Many lithium containing ores and concentrates are rather simple in mineralogical composition and are often based on binary mineral assemblages. Using these compositions in binary and ternary mixtures of lithium minerals, such as spodumene, amblygonite, lepidolite, zinnwaldite, petalite and triphylite, a quantification of mineral content can be made. The recalculation of lithium content from quantitative mineralogical analysis leads to a fast and reliable lithium determination in the ores and concentrates. The techniques used for the characterization were quantitative mineralogy by the Rietveld method for determining the quantitative mineral compositions and statistical calculations using additional methods such as partial least square regression (PLSR) and cluster analysis methods to predict additional parameters, like quality, of the samples. The statistical calculations and calibration techniques makes it especially possible to quantify reliable and fast. Samples and concentrates from different lithium deposits and occurrences around the world were used for these investigations. Using the proposed XRD method, detection limits of less than 1% of mineral and, therefore down to 0.1% lithium oxide, can be reached. Case studies from a hard rock lithium deposit will demonstrate the value of mineralogical monitoring during mining and the different processing steps. Additional, more complex considerations for the analysis of lithium samples from salt lake brines are included and will be discussed.

Keywords: lithium; quantification; XRD; PLSR; clustering; Rietveld; cluster analysis; spodumene; petalite; lepidolite; triphylite; zinnwaldite; amblygonite



Citation: Pöllmann, H.; König, U. Monitoring of Lithium Contents in Lithium Ores and Concentrate-Assessment Using X-ray Diffraction (XRD). *Minerals* **2021**, *11*, 1058. <https://doi.org/10.3390/min11101058>

Academic Editor: Fang Xia

Received: 22 July 2021

Accepted: 14 September 2021

Published: 28 September 2021

Publisher's Note: MDPI stays neutral with regard to jurisdictional claims in published maps and institutional affiliations.



Copyright: © 2021 by the authors. Licensee MDPI, Basel, Switzerland. This article is an open access article distributed under the terms and conditions of the Creative Commons Attribution (CC BY) license (<https://creativecommons.org/licenses/by/4.0/>).

1. Introduction

Lithium is an element in the chemical periodic system with ordinal number 3. The formation and details on the metal are summarized by [1–5]. Almost half of the lithium production is nowadays increasingly used in the fabrication of batteries [5,6]. Therefore, an increasing demand in the metal supply is visible [7,8]. Other uses of lithium are in ceramics industry, grease, polymers and air treatment among others. The main lithium resources are coming from lithium salt lake brines in arid areas and from different lithium containing minerals, often concentrated in economic mining sites [9–13]. Lithium resources in Europe were summarized by [14]. The worldwide situation was described by [15–17]. Some lithium containing clays are also promising nowadays. Lithium forms 124 mineral species [18,19]. 44% of all lithium minerals occur in LCT-pegmatites and associated metasomatic rocks [20,21]. Other main sources of lithium minerals are non-LCT pegmatites and

their metasomatic rocks, metasomatic rocks not associated with pegmatites, and manganese deposits [19]. A list of widely abundant minerals is given in [18]. However, not all of these are enriched in quantities to be mined. The mineral with the highest lithium-content is the rare Zabuyelite Li_2CO_3 (18.79%). A summary of lithium demand and supply is given in [22]. By analyzing elements associated in LCT pegmatites (LCT = lithium-cesium tantalum pegmatites) [23] (Ga, Rb, Nb, Sn, Cs, Ta, Tl) satisfactorily lithium can be predicted [24] by μ -XRF. Another basis for lithium is also the occurrence in salt lakes in dry areas. The lithium must be concentrated by thermal and leaching processes [25–30]. A review of enrichment techniques is given by [31]. Some investigations are included in this publication. Li-Minerals, which can be mined in large quantities, as a basic source from geological enrichment with their chemical compositions and XRD data files, are summarized in Table 1. The lithium determination in these mineral concentrates will be described.

Table 1. Important lithium-bearing minerals, compositions and crystal structure files.

Mineral	Composition	Lithium-Content in wt. %	Lithium Oxide Content in wt. %	ICSD-No.	Literature
Spodumene	$\text{LiAl}[\text{Si}_2\text{O}_6]$ —(α , β , γ)	3.73	8.03	30,521 9668 (α) 14,235 (β) 69,221 (γ) Virgilite	[32]
Petalite	$\text{LiAl}[\text{Si}_4\text{O}_{10}]$	3.09	4.50	100,348	[33]
Lepidolite Polyolithionite	$\text{KLi}_2[\text{AlSi}_3\text{O}_{10}/(\text{OH},\text{F})_2]$	3.58 3.00	7.7 6.46	30,785 34,336 (with F)	[30]
Zinnwaldite	$\text{KLiFeAl}[\text{AlSi}_3\text{O}_{10}/(\text{F},\text{OH})_2]$		3.42	432,226	[34]
Amblygonite/ Montebrasite	$\text{LiAl}[\text{PO}_4\text{F}]/$ $\text{LiAl}[\text{PO}_4\text{OH}]$	3.44/3.80 4.74	10.21 7.49 (at 5% Na_2O)	26,513 68,925 (OH/F) 68,921 (OH)	[18]
Lithiophilite/ Triphylite	$\text{LiMn}[\text{PO}_4]/$ $\text{LiFe}[\text{PO}_4]$	4.43 4.40	9.53 9.47	75,283 72,545	[35]

For these lithium minerals from definite occurrences, different calibration curves were set up and statistical methods were successfully introduced to determine the relevant lithium oxide content of these mixtures. The lithium content of these Li-minerals increases from Zinnwaldite, Petalite, Lepidolite, Spodumene, and Triphylite to Amblygonite/Montebrasite. It must also be taken into account that these minerals can form solid solutions which do influence these absolute lithium contents and must be adapted and determined separately [36]. In Figure 1 the theoretical calibration curves of the six lithium containing minerals, with ideal composition, showing their maximum lithium contents, are given. In practical work these curves with the lithium contents of the respective occurrence must be adapted due to the investigated mineral composition and ore compositions from different geological occurrences.

The used lithium minerals in this study come from different origins. These determined compositions can be representative for other occurrences, but must otherwise simply be adapted, mainly when different solid solutions of these minerals do occur. For all calibrations, the standard mineral compositions of the relevant occurrences were used. Calibrations must be changed when larger differences in mineral compositions occur. The used lithium ores and their matrices can be seen in Figure 2a–f showing the different lithium minerals coming from varying origins. These used ores and concentrates are rather simple in mineralogical compositions as mineral paragenesis for these processed ores are very uniform. Many of these ores are only composed of additional quartz, and some also contain feldspar.

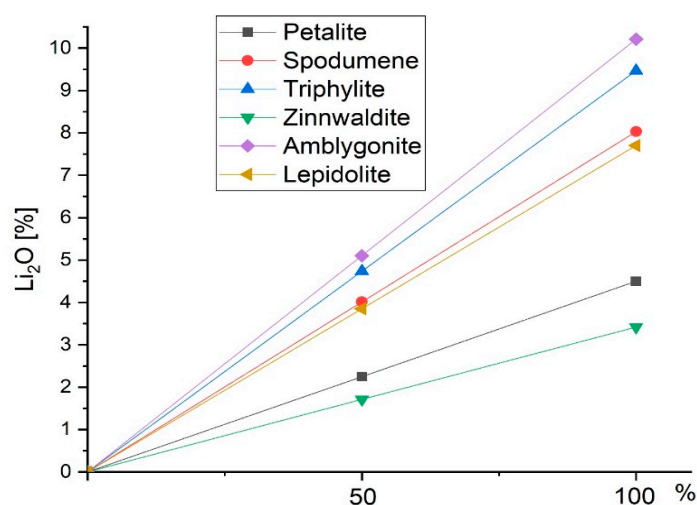


Figure 1. Maximum lithium oxide contents in different lithium minerals. Variation of lithium depending from content of the minerals (wt.%).

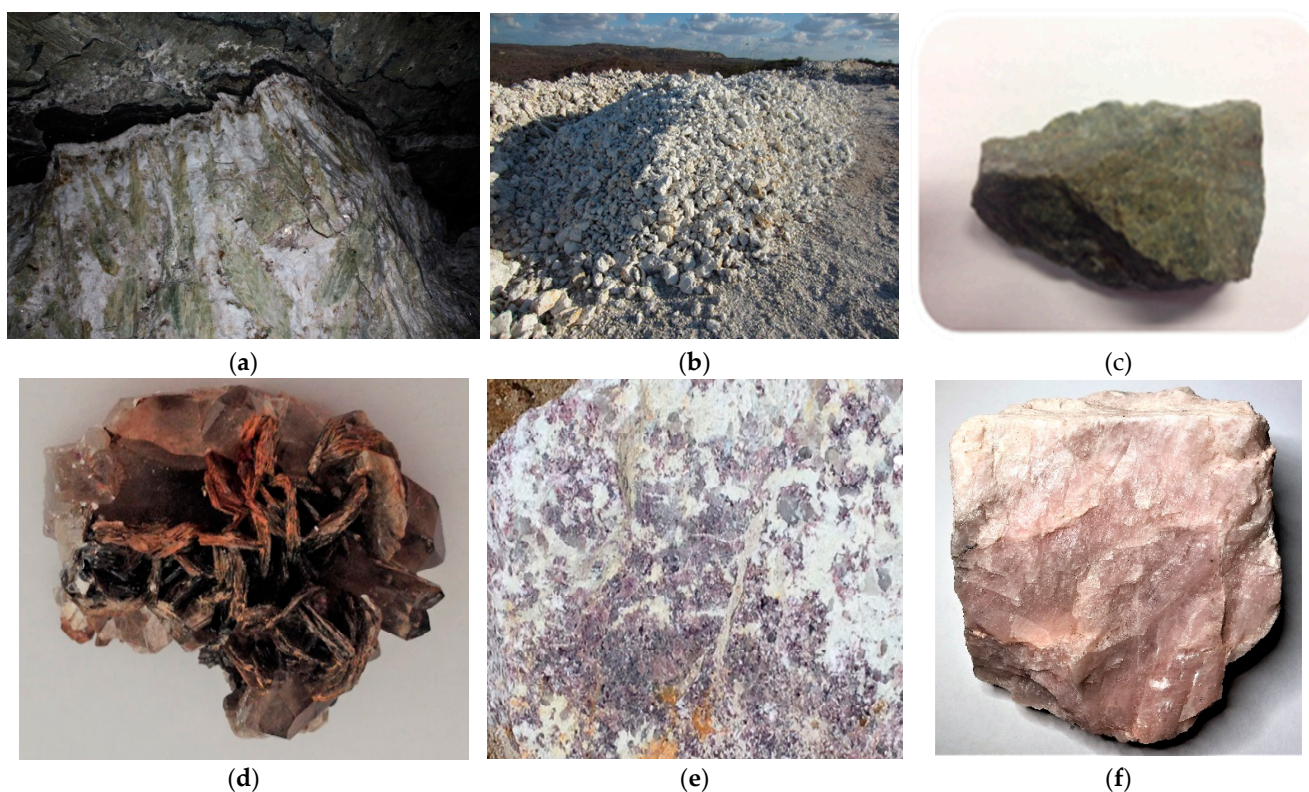


Figure 2. (a) Underground image of slightly green spodumene crystals (green crystal size ca. 1 m) in quartz matrix—MG—Brazil, (b) Montebrasite/Amblygonite occurrence with quartz—Serra Branca, Brazil, image: 30 m, (c) Triphylite with small quartz intergrowth—Hagendorf, Germany, image: 10 cm, (d) Zinnwaldite mica—Ore mountains/Germany, image: 5 cm, (e) Lepidolite in quartz/feldspar assemblage—Mangualde, Portugal, image: 10 cm, (f) Petalite/Rubicon mine—Namibia, image: 10 cm.

The lithium contents of the minerals must be carefully calculated due to their chemical compositions. Spodumene, petalite and triphylite minerals are easy to handle since their solid solutions are rather restricted. For Montebrasite/Amblygonite, Zinnwaldite and Lepidolite, the lithium contents must be determined in advance, since different solid solutions of these minerals may occur in different occurrences.

For all determinations it is also necessary to verify these contents from time to time, as some change may also be possible in the geological surroundings within one occurrence.

2. Experimental

A technical approach for lithium determination by quantitative mineral determination and following Li_2O calculation was performed using XRD powder techniques and different interpretation methods. Due to the non-possibility of a direct XRF analysis for lithium, a new method based on quantitative X-ray Diffraction of the lithium minerals, combined with calculation of lithium from their mineralogical composition, is proposed. Time-consuming wet chemical analysis procedure is only used from time to time for verification purposes. The following XRD techniques and combined calculating statistical procedures were applied for these quantitative mineral and lithium determinations:

2.1. Qualitative and Quantitative Mineral Analysis by XRD Combined with Rietveld Refinement Calculations

The XRD analysis was performed using a PANalytical Expert system (Panalytical Highscore Version 4.9, Almelo, The Netherlands) with X'celerator detector and program Highscore Plus for analytical treatment of qualitative mineral compositions. Mineral determinations were done by using the actual ICDD (PDF4, 2021) (International Centre for Diffraction Data, Newtown Square, PA, USA) database. Also, the same program was used for Rietveld [22,37] refinement and statistical procedures. The relevant ICSD (Inorganic Crystal Structure Database, FIZ Karlsruhe) structure files are summarized in Table 1. The sample preparation for XRD was conducted by filling fine milled powders into steel ring sample holders using the backload preparation methodology.

The following parameters for X-ray experiments were used (Table 2).

Table 2. XRD measurement parameters. (LFF = long fine focus spot).

Parameter	LFF-Tube-Cu	LFF-Tube-Co
Measurement range (2 theta)	5–70	5–90
Step (2 theta)	0.02	0.02
Counting time in s	10	10
Antiscatter slit	1/8	1/8
Soller slits	2.3	2.3
Voltage in kV	45	40
Tension in mA	30	35
β -filter	Ni	Fe

Quantitative analysis of the samples was mainly made using Rietveld analysis in Highscore Plus program. Quantification of amorphous contents was made by the addition of an Inner standard (Rutile) of 10%. Background calculation was added as determined manually. Refinement control of the samples was performed using the Pseudo-Voigt profile function, scale factor, zero shift, unit cell and W-profile parameter. The verification of the determined contents was obtained by addition of definite amounts of mineral phases and following calculations and construction of the regression curves.

2.2. PLSR—Partial Least Squares Refinement Techniques for Different Mineral Mixtures

Full pattern Rietveld quantification [2,8,38,39] using crystal structures can be replaced by partial least squares refinement calculations using high score plus platform and the specific part of the program for correlating mineral contents and XRD results. The PLSR can be mainly used also in industrial applications to correlate mineral components with their quantitative contents. With this method no pure phases, crystal structures or modelling of peak shapes are necessary. For setting up this method a number of samples for calibration and validation are needed. Data are afterwards processed by calculating diagrams showing regression plots of reference values (X-axis) versus predicted values (Y-axis). Different

scaling mode methods can be used to find the best calibration model (center method (the mean is subtracted from each value for the definite variable) and standardize method (the variables are standardized by subtracting the mean and dividing by the standard deviation). After calibration these models can be used for unknown samples to predict the defined property. With the used equipment, a precise result can be obtained within minutes and therefore the method can be used for process control. No specific preferred orientation refinement model was used, as this can influence the content of the minerals. Instead, for the calibration the preparation was standardized.

2.3. Cluster-Analysis of Obtained XRD Patterns of Mixtures

Cluster analysis is a statistical method [2,40–42] which can be used for obtaining rapid results in ore assessment by finding similar groups (clusters) which are more similar to each other than to those of other groups. The technique is mainly used for data reduction. It is applied here to find clusters containing similar grades of lithium contents in the ores (high, intermediate, and low grade) to obtain arguments for further ore treatment. Within this method additional possibilities can be used for further optimizations (PCA (principal component analysis), dendrogram, KGS (Kelley, Gardner, Sutcliffe) test and others). The dendrogram is a possibility to define different clusters using the cut off between less similar XRD patterns. Mainly, cluster analysis is used for data reduction of complex systems.

2.4. Principal Component Analysis—PCA

PCA plots [40,43] using the resulting eigenvectors, can create a three-dimensional arrangement of first three principal components and can show thereof the XRD data belonging to the different clusters.

2.5. Determination of Detection Limits for Different Lithium Minerals in Matrices

The minimal detection of minerals in the relevant matrices is the basic fact that must be done to see what is the lowest lithium concentration which can be detected. Despite these low concentrations not being as interesting as lithium ores, these mixtures can be classified in the different group of low content lithium ore or otherwise a different fourth grade can be added, meaning low lithium contents without any interest for lithium extraction. The lowest lithium concentration which can be measured is dependent on the possibility of identifying the lithium mineral in the matrix and is given for any lithium mineral used in this study.

Furthermore, the program High Score Plus was used for Rietveld refinement and some additional statistical procedures. The relevant ICSD structure files necessary for Rietveld analysis are summarized in Table 1.

For these investigations of lithium content determinations in lithium concentrates different localities with several relevant lithium minerals from deposits in Germany, Portugal, Namibia, Brazil, Finland, and Australia were used. The results for these 6 main important lithium minerals, ores and concentrates are presented. Different additional interesting results were obtained for complex analyses of multi-mineral lithium brine investigations originating from Chile.

3. Results for the Quantifications of Different Lithium Minerals in Binary Mixtures with Quartz

3.1. Quantification of Petalite— $\text{LiAlSi}_4\text{O}_{10}$ —Quartz SiO_2

Petalite ore samples from the Namibian occurrence were used in a typical binary mixture with quartz and 10% of weight differences were used. These samples were used to determine the mineral contents and thereof the lithium contents. A calibration curve for Petalite [33] with different amounts (10% weight portions) of accompanying quartz was set up using XRD's with different contents of the minerals (Figure 3). It can easily be seen, that high and medium grade ores (contents of 100 weight% to 20 weight% Petalite) show strong Petalite peaks in XRD patterns, which can easily be identified.

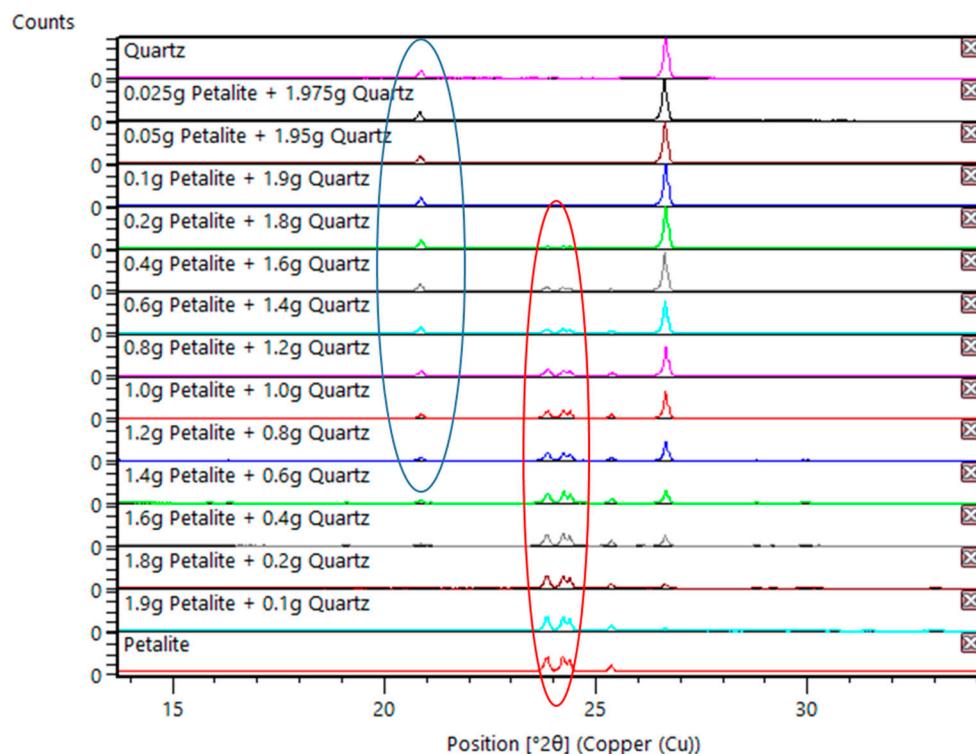


Figure 3. XRD patterns used for the calibration of petalite–quartz weight% mixtures (triplet of petalite peaks and main peak of quartz highlighted).

In the mixtures also the minimum content of the lithium mineral petalite, which can be detected, was determined. In Figure 4 the XRD patterns of pure petalite and a mixture of quartz with 5% of petalite is shown. Figure 4b shows several XRD patterns of binary mixtures and also the binary mixture at the detection limit of Petalite in a quartz matrix. It can be seen, that the main peak of petalite is easily detectable, meaning, that lithium contents down to 0.5% Li₂O can be detected. In Figure 5 the linear calibration curve using PLSR curves of petalite in quartz matrix is given.

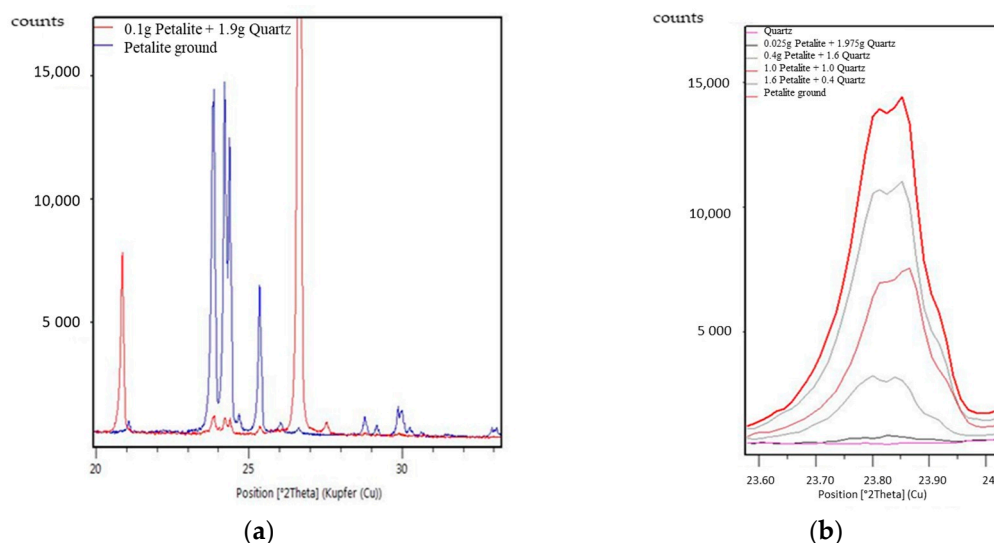


Figure 4. Determination limit of petalite in quartz matrix using main peaks of petalite. (a) Part of XRD pattern petalite and mixture of 95% quartz/5% Petalite; (b) Main peak of petalite in quartz matrices of different contents.

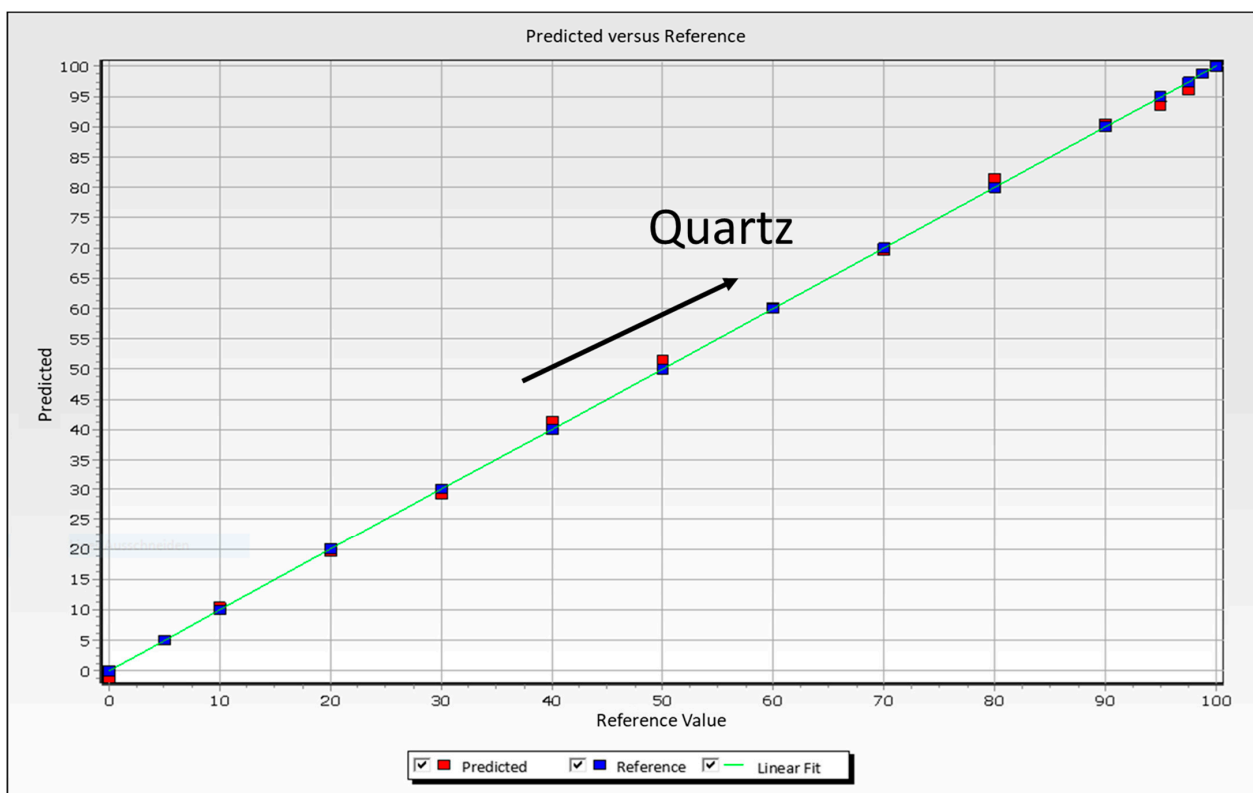


Figure 5. PLSR calibration curve for petalite–quartz mixtures.

From these different contents of petalite in lithium mineral quartz matrix the detection limit for lithium oxide can be derived (Table 3) showing the contents of lithium oxide derived from XRD patterns in Figure 4b. The PLSR calibration curve for petalite–quartz mixtures is given in Figure 5.

Table 3. Lithium oxide content as given from several selected petalite/quartz mixtures.

XRD-Mixture of Petalite/Quartz in %	Li ₂ O Content in %
Petalite 100	4.5
Petalite/Quartz 80/20	3.6
Petalite/Quartz 50/50	2.25
Petalite/Quartz 20/80	0.9
Petalite/Quartz 1.25/98.75	0.056

The cluster analysis brings similar contents of minerals into selective groups when necessary. Segments of three different clusters, containing areas with comparable lithium contents (high-medium-low grade ores) were determined in this case (Figure 6), but it is also possible to calculate other different clusters (and derived lithium contents thereof) in application cases when necessary. Here it is possible to determine for instance cut off values of economic lithium mineral contents.

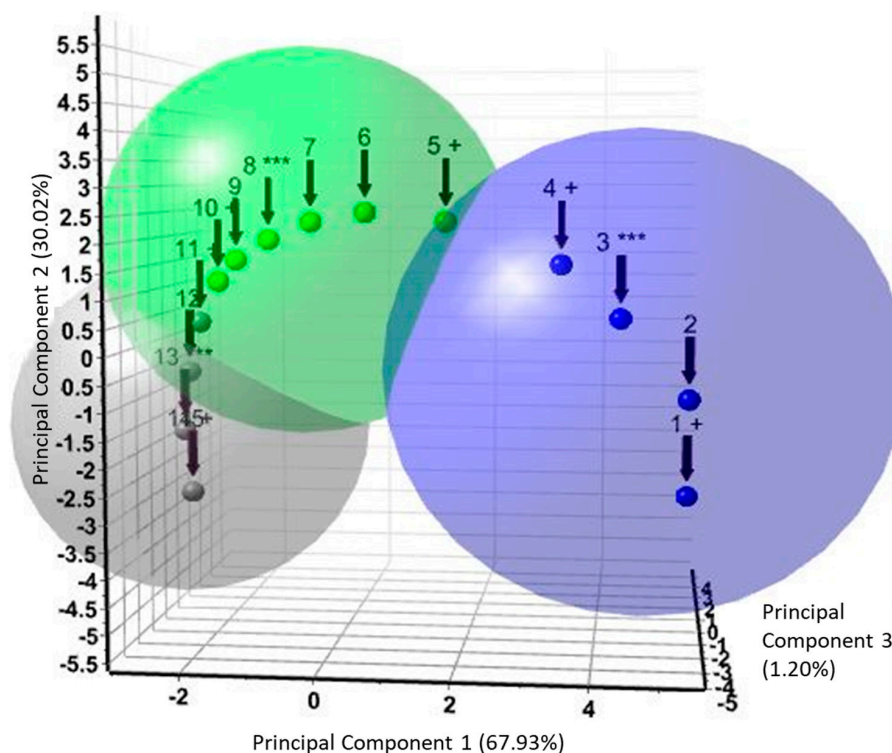


Figure 6. Clustering of petalite–quartz mixtures (three clusters with differing lithium contents). *** most representative sample of cluster, + are the most different ones in the clusters.

3.2. Quantification of Spodumene $LiAlSi_2O_6$ -Quartz SiO_2

As spodumene is an important lithium mineral [32,44] some determinations on rather pure ores and concentrates were made. The results of the XRD calibration measurement of spodumene and quartz mixtures from Brazilian occurrence are summarized in Figure 7. The main peaks of spodumene and quartz are highlighted, to verify, that precise identifications of minerals can be made rather easily. The PLSR calibration curve for mixtures of spodumene and quartz is shown in Figure 8.

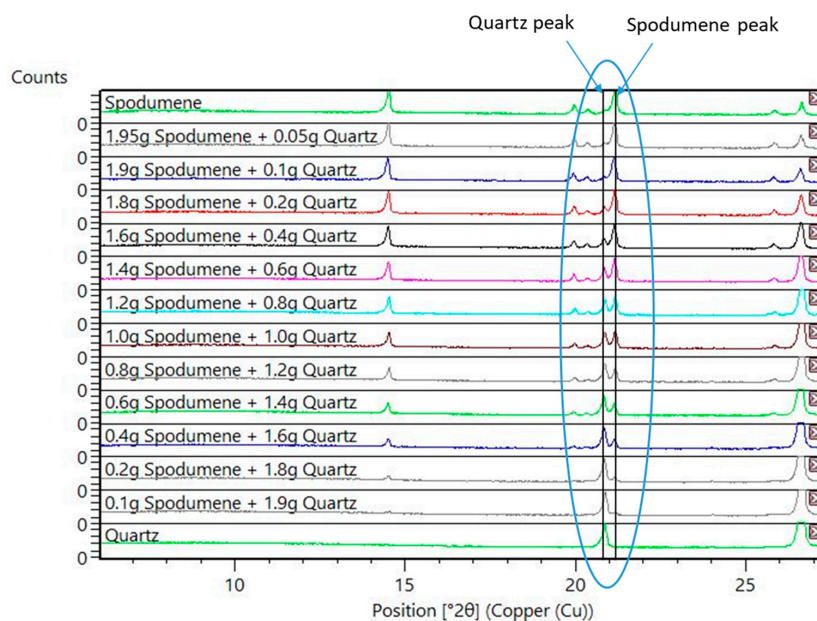


Figure 7. XRD patterns of different spodumene–quartz mixtures (main peak of quartz and spodumene highlighted).

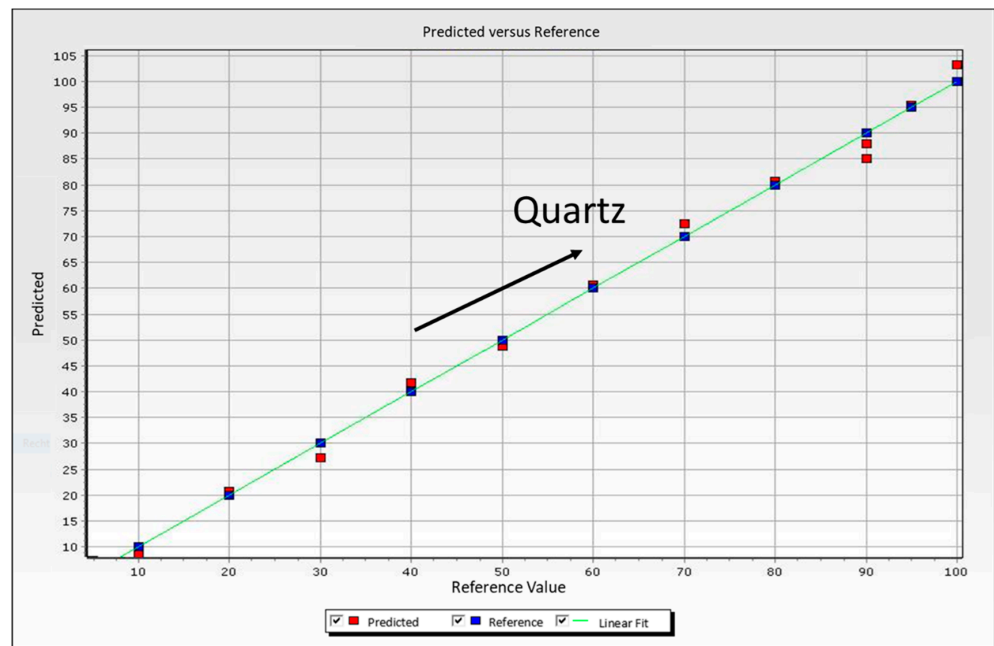


Figure 8. Calibration curve for spodumene–quartz mixtures.

As an example for Rietveld refinement control of the different mixtures, the Rietveld plot for a mixture of 95% spodumene and 5% of quartz and the calculated composition is given in Figure 9.

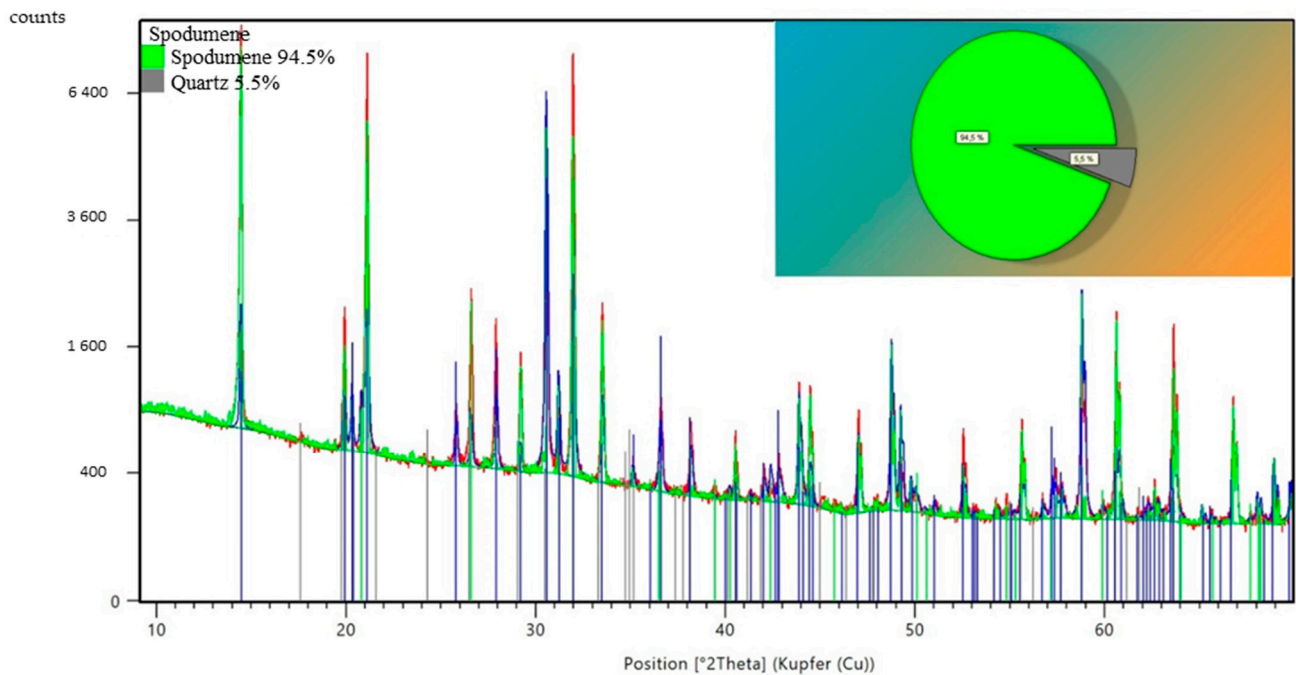


Figure 9. Rietveld refinement of a spodumene–quartz mixture.

It is also possible to cluster these spodumene containing mixtures in three different lithium grade ores as given in Figure 10 (low, medium, and one high lithium containing grade). The detection limit of spodumene was also determined.

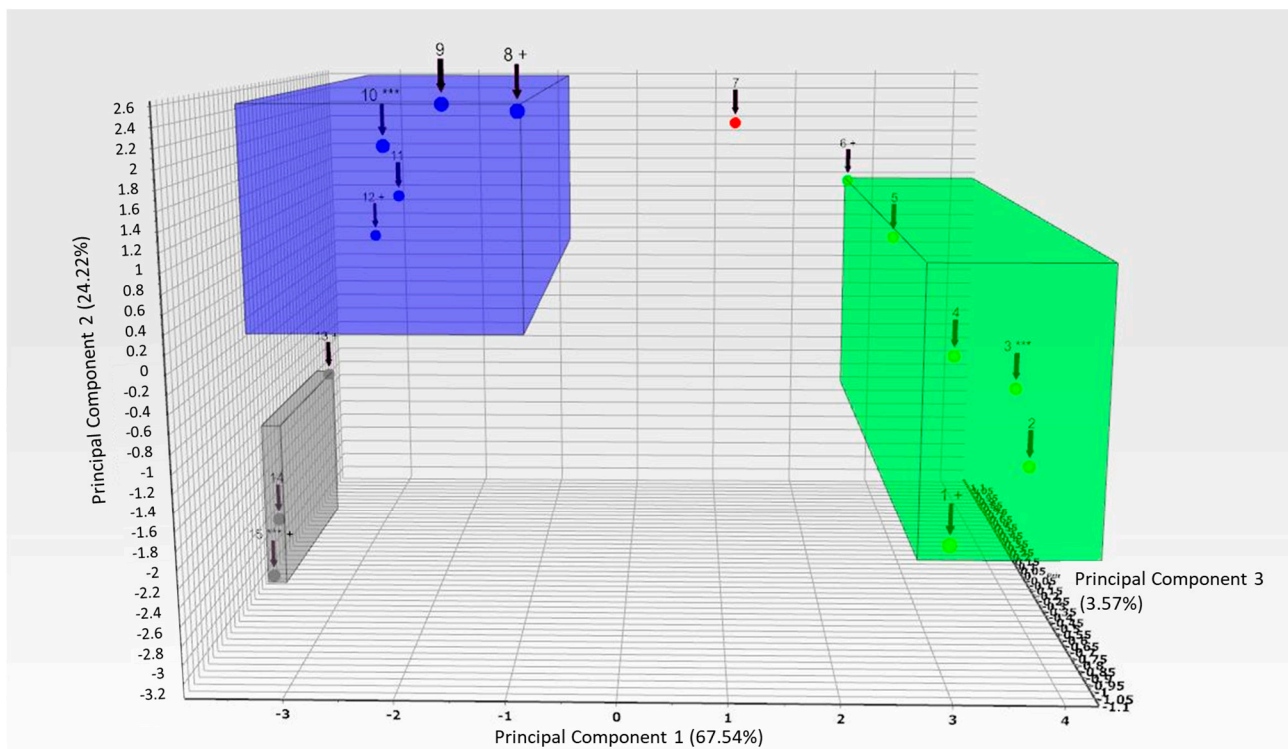


Figure 10. Clustering of spodumene–quartz mixtures (three clusters with different lithium contents). *** most representative sample of cluster, + are the most different ones in the clusters.

3.3. Quantification of Triphylite LiFePO_4 -Quartz SiO_2

Investigations using Triphylite (LiFePO_4) (Hagendorf/Bavaria) [36] ore must primarily deal with the possible solid solution with Lithiophorite (LiMnPO_4). This composition for the geological occurrence is definitely used for making the calibration curves. Figure 11 shows the PLSR calibration curve for triphylite–quartz mixtures for a typical Hagendorf lithium ore.

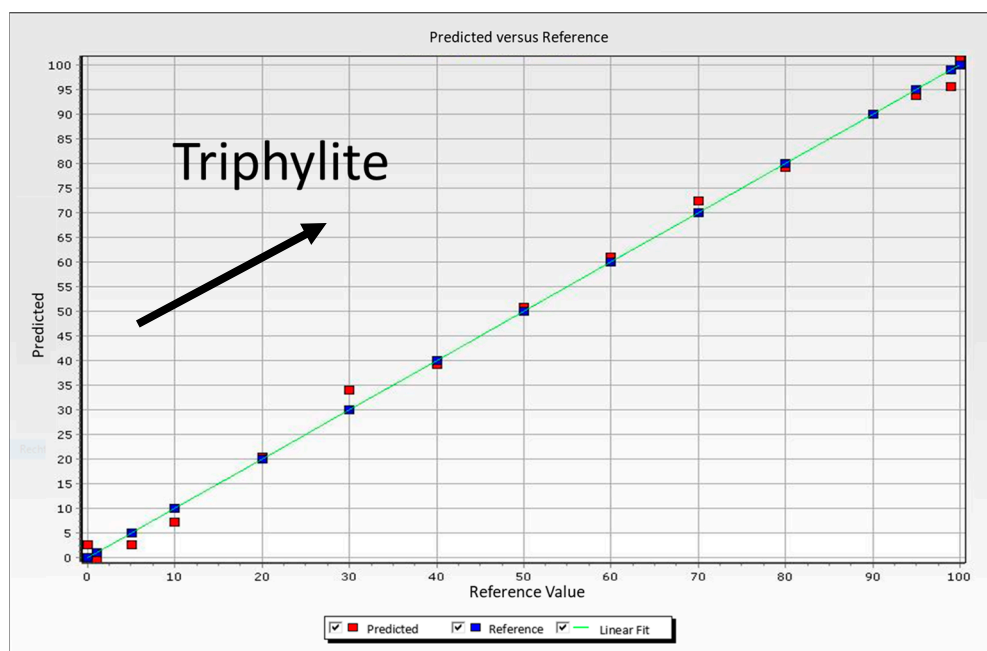


Figure 11. Calibration curve for triphylite–quartz mixtures.

The different mixtures were additionally clustered into four different triphylite containing lithium mineral mixtures (Figure 12). The detection limit for triphylite in quartz mixtures and the lithium content of these ores was determined as well (Figure 15).

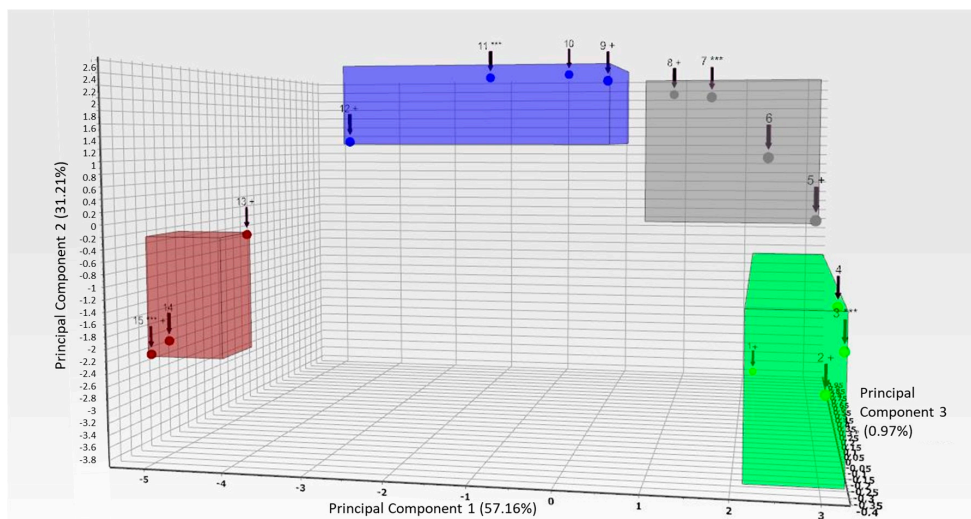


Figure 12. Clustering of triphylite–quartz mixtures showing four different lithium ore grades. *** most representative Scheme 2. contents, low triphylite, medium triphylite, and high triphylite contents. The XRD patterns of these mixtures and their calculated groups, including their similarities, are given in Figure 14. To show the relevant main peaks of the mineral quartz in these mixtures, with special emphasis to low amounts, Figure 15 is added.

The graphical way to determine detection limits of triphylite is given in Figure 13 by showing the relevant XRD patterns of quartz–triphylite mixtures. 1% of triphylite in a quartz matrix can easily be determined in these mineral mixtures.

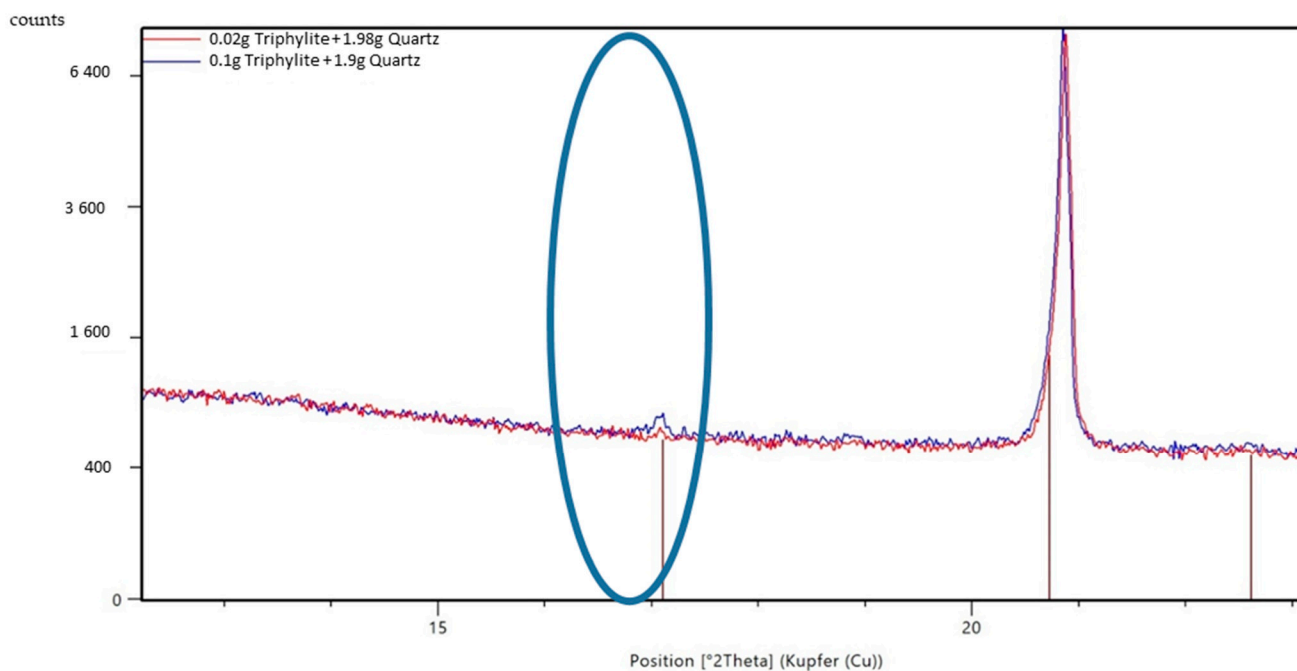


Figure 13. XRD pattern of small additions of triphylite to quartz matrix (1% Triphylite/99% Quartz).

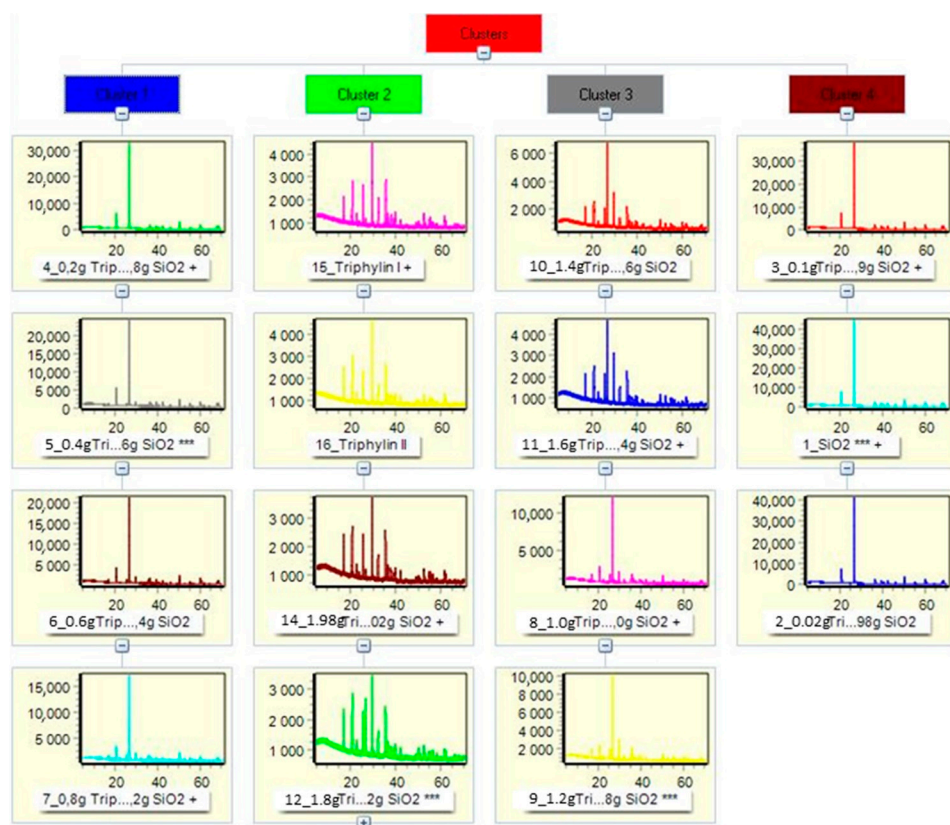


Figure 14. XRD patterns belonging to the respected determined clusters with different triphylite–quartz contents.

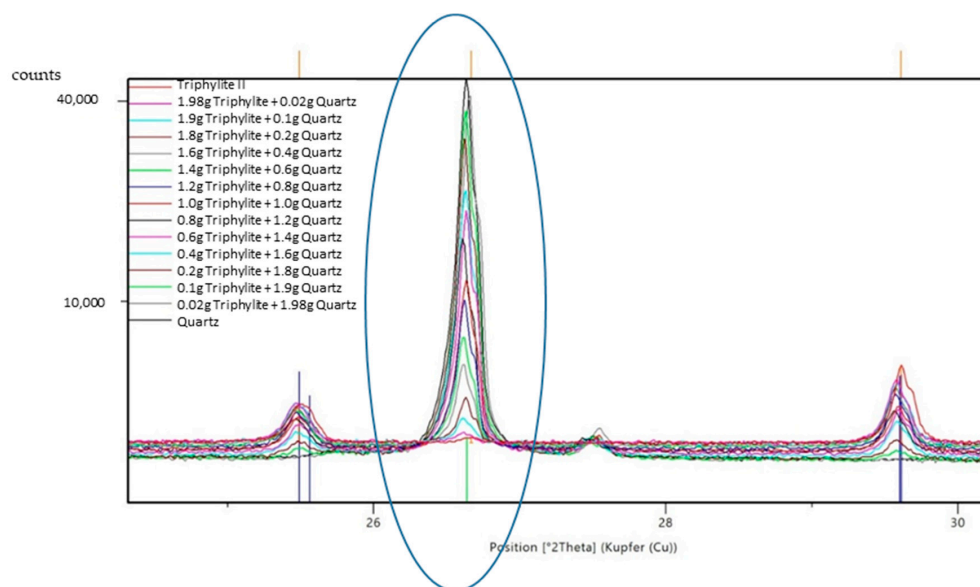


Figure 15. Main peak of quartz in triphylite–quartz calibration mixtures.

3.4. Quantification of Montebasite $\text{LiAlPO}_4(\text{OH},\text{F})\text{-Quartz SiO}_2$

For the determination of different montebasite (F-containing) contents from NE-Brazil in the mixtures with quartz a calibration curve using PLSR was set up. The derivation of this method must also include the solid solution of the minerals montebasite and Amblygonite [45]. The XRD patterns of montebasite/quartz mixtures are shown in Figure 16 and the PLSR calibration curve for montebasite is given in Figure 17.

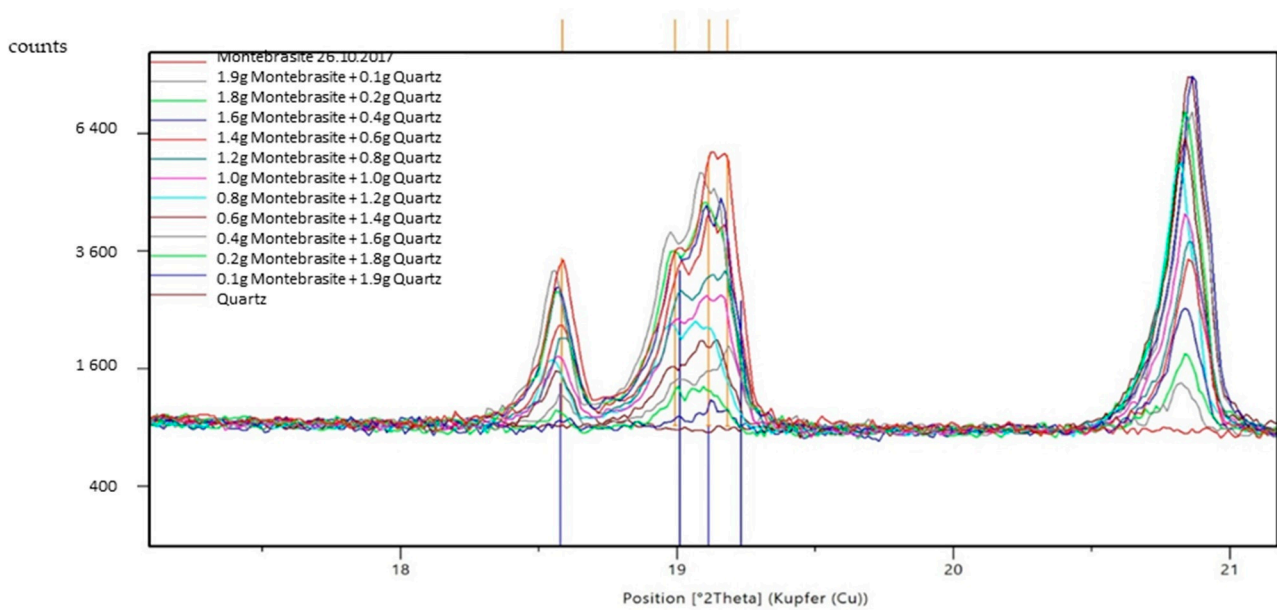


Figure 16. XRD patterns showing different contents of montebrasite–quartz mixtures.

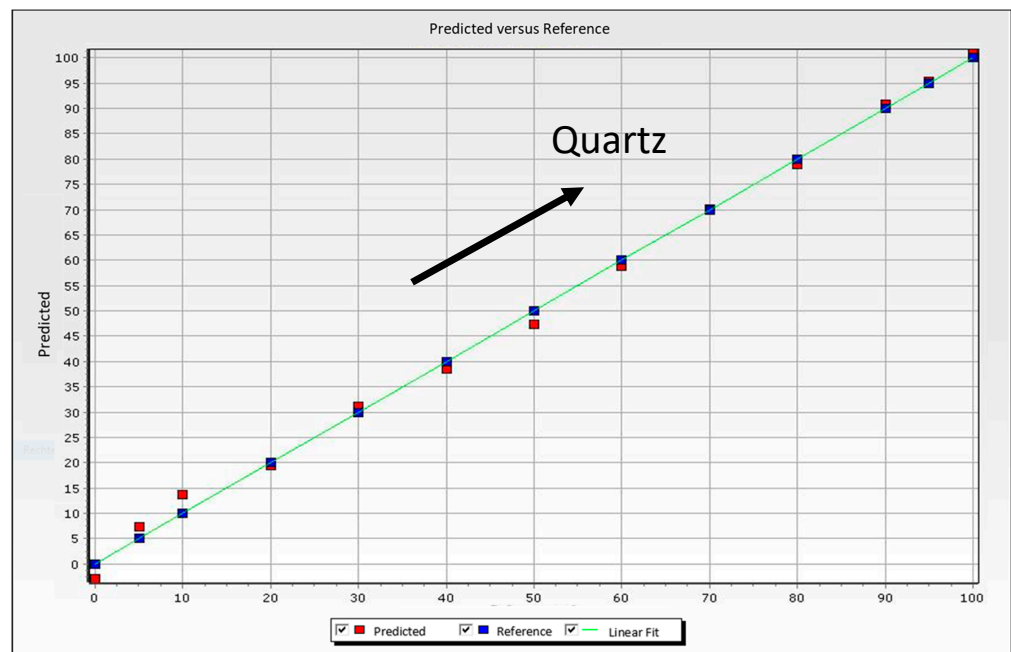


Figure 17. Calibration curve for montebrasite–quartz mixtures.

The clustering of XRD scans revealed four clusters of (a) SiO_2 -rich, (b) Montebrasite-rich, (c) intermediate Montebrasite, and (d) intermediate SiO_2 -contents (Figure 18).

The following cluster details showed the different XRD patterns which compose these separated four clusters with different montebrasite contents (high, medium, medium low, low) (Figure 19).

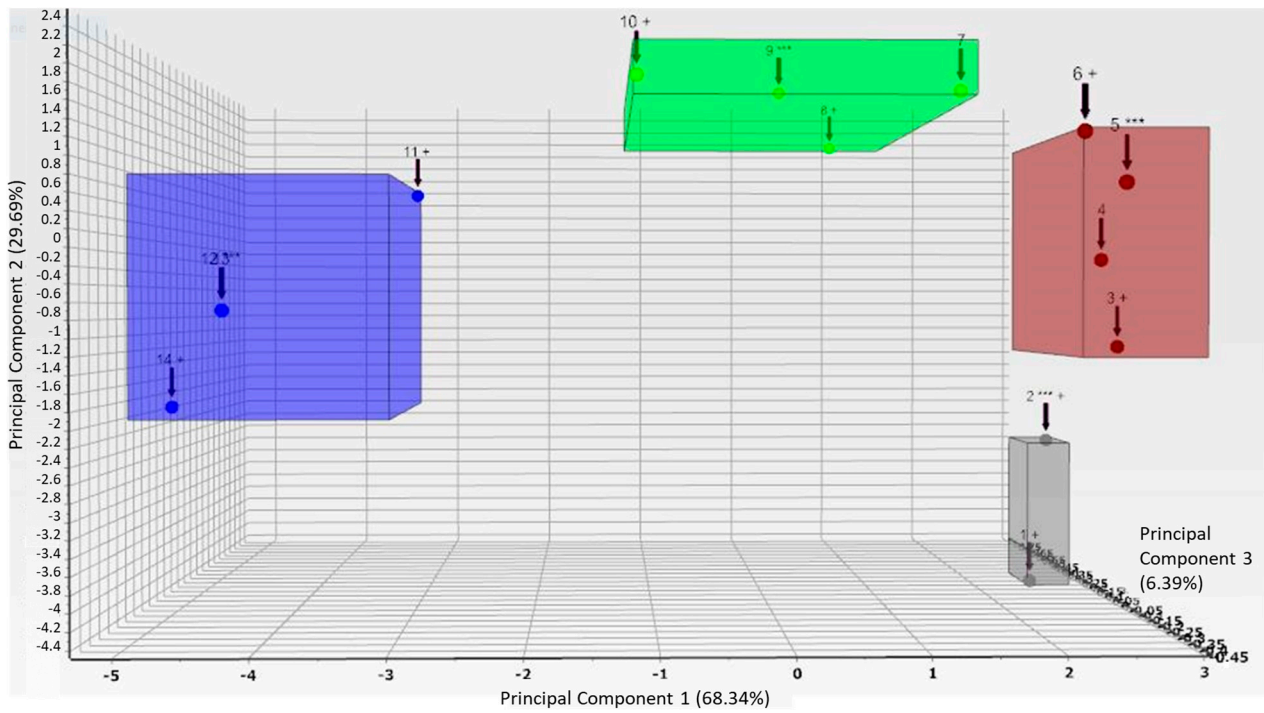


Figure 18. Clustering of montebasite–quartz XRD diagrams. *** most representative sample of cluster, + are the most different ones in the clusters.

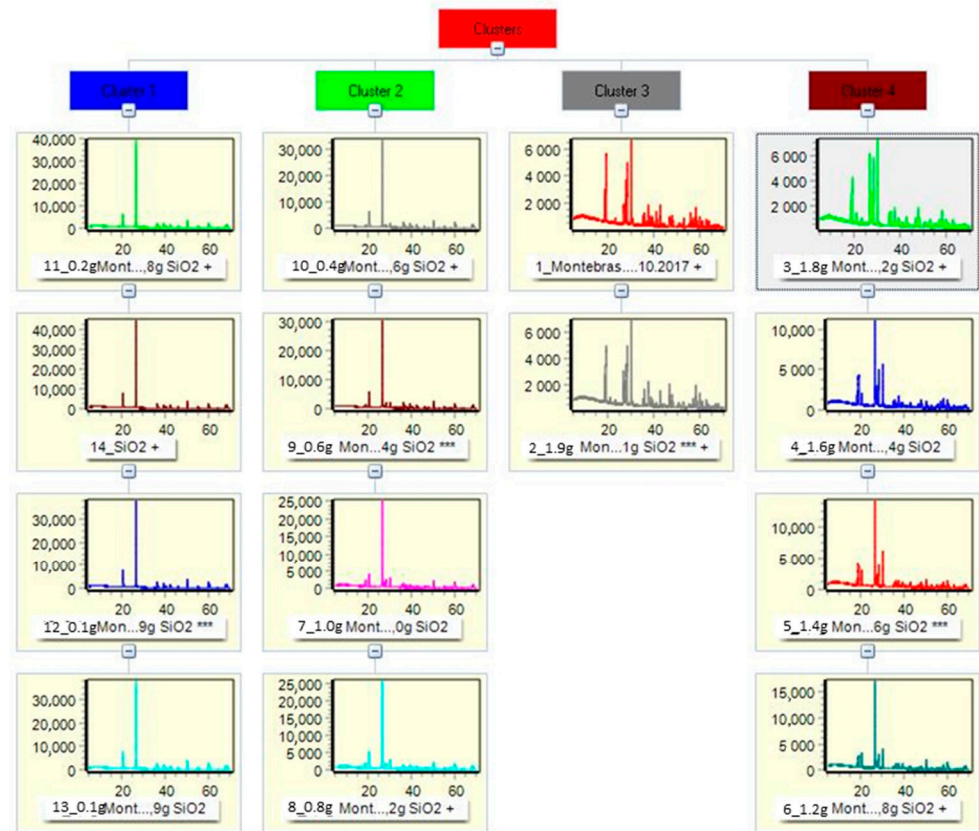


Figure 19. XRD patterns of quartz–montebasite mixtures forming the four relevant calculated clusters.

3.5. Quantification of Lepidolite $KLi_2AlSi_3O_{10}(OH,F)_2$ -Quartz SiO_2

For the calibration of lepidolite mica and quartz some samples from Portugal were used. For micas the preparation must be done very carefully to obtain a comparable kind of preferential orientation in all samples, as this can influence the intensity of the peaks. Especially for small amounts of mica, a highly preferential orientation can be included to increase the determination limit. The intensity of a main peak of lepidolite in the mixtures with quartz is given in Figure 20. The calculated PLSR calibration curve for lepidolite is given in Figure 21.

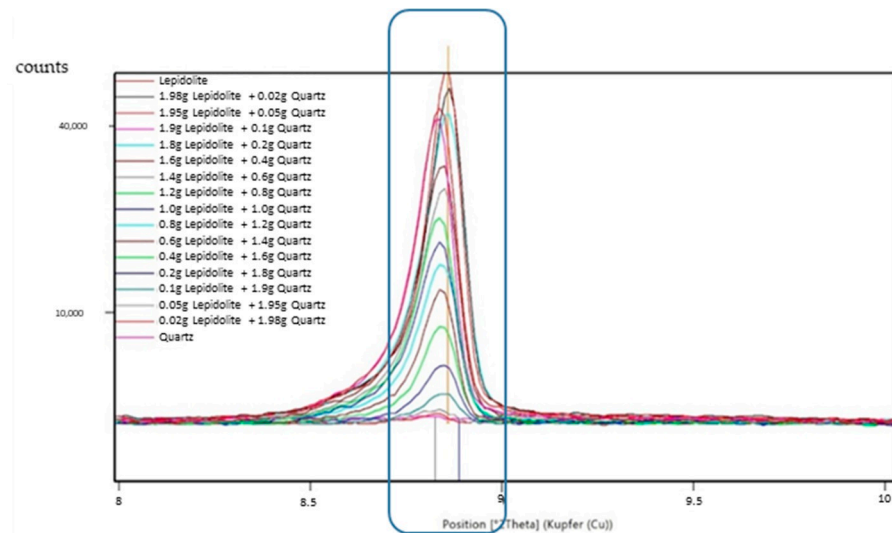


Figure 20. Details of XRD patterns showing main peak of lepidolite in different contents.

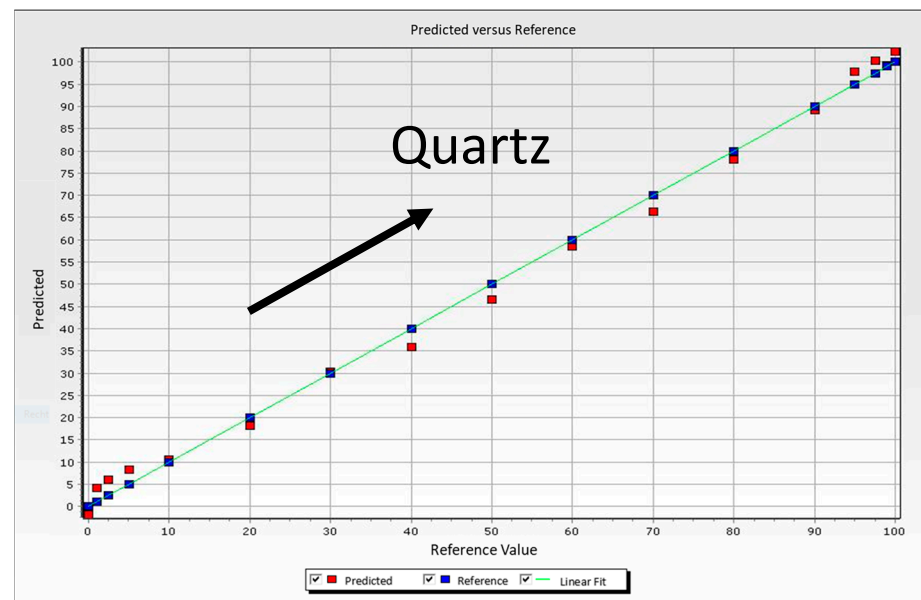


Figure 21. Calibration curve for lepidolite–quartz mixtures.

The results of the clustering into four lepidolite containing clusters and the relevant XRD patterns are given in Figures 22 and 23.

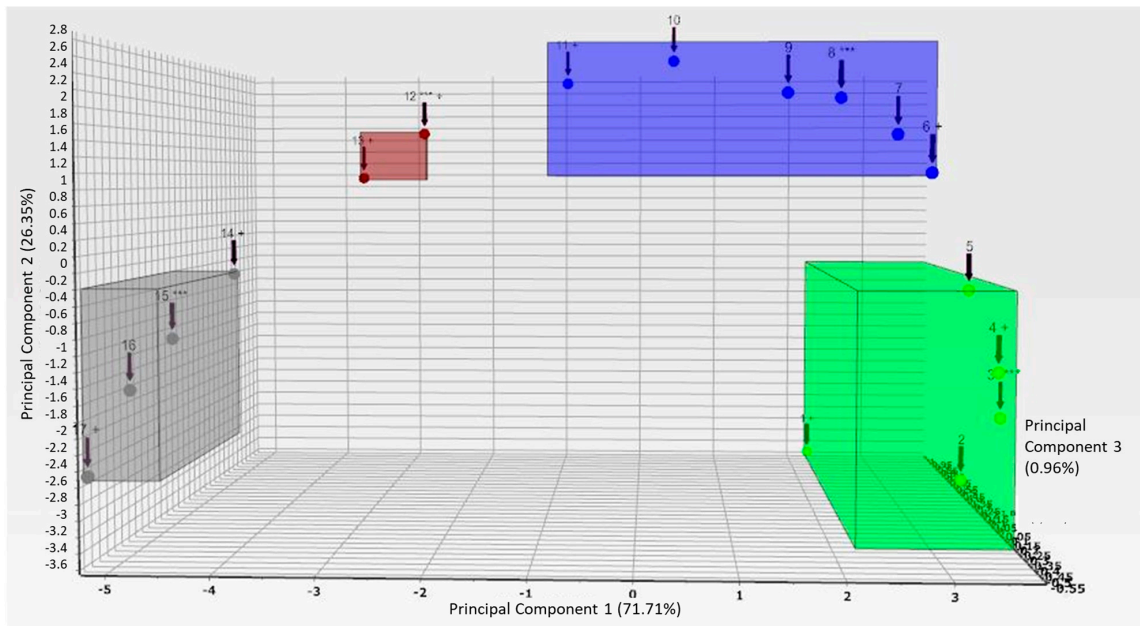


Figure 22. Clustering of XRD patterns of lepidolite–quartz mixtures. *** most representative sample of cluster, + are the most different ones in the clusters.

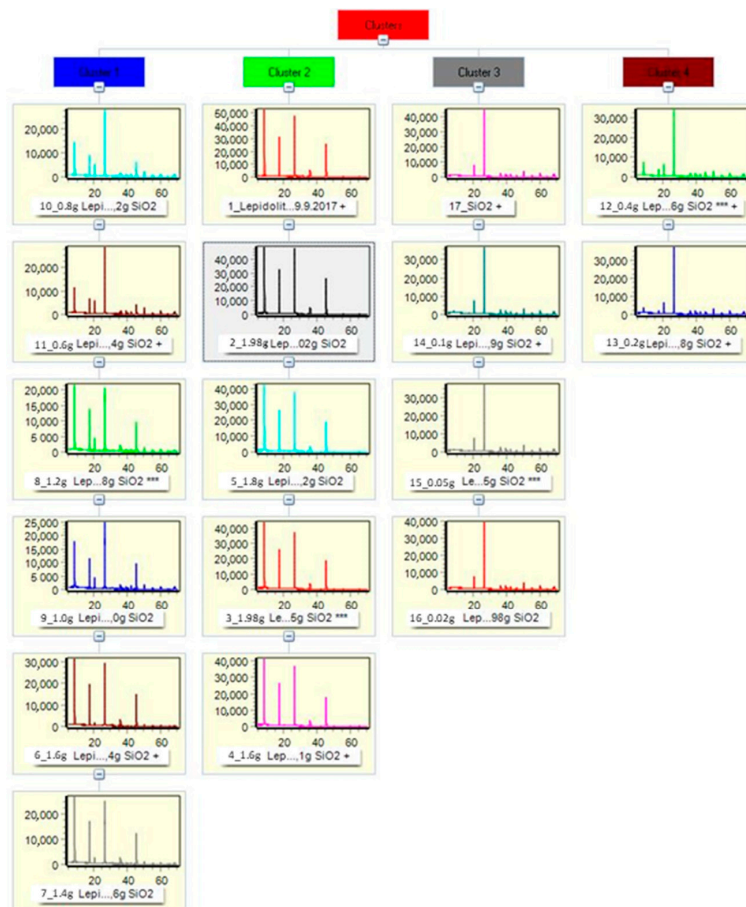


Figure 23. XRD patterns of quartz–lepidolite mixtures forming the relevant calculated clusters.

3.6. Calibration of Zinnwaldite $KLiFeAl_2Si_3O_{10}(F,OH)_2$ -Quartz SiO_2

Using zinnwaldite [35] as a lithium source the same precautions in the preparation of XRD patterns as in lepidolite case for micas must be used controlling the preferential orientation of mica platelets. Typical XRD patterns showing varying contents of quartz and zinnwaldite peak areas are given in Figure 24. The calculated PLSR calibration curve for zinnwaldite-quartz mixtures is given in Figure 25.

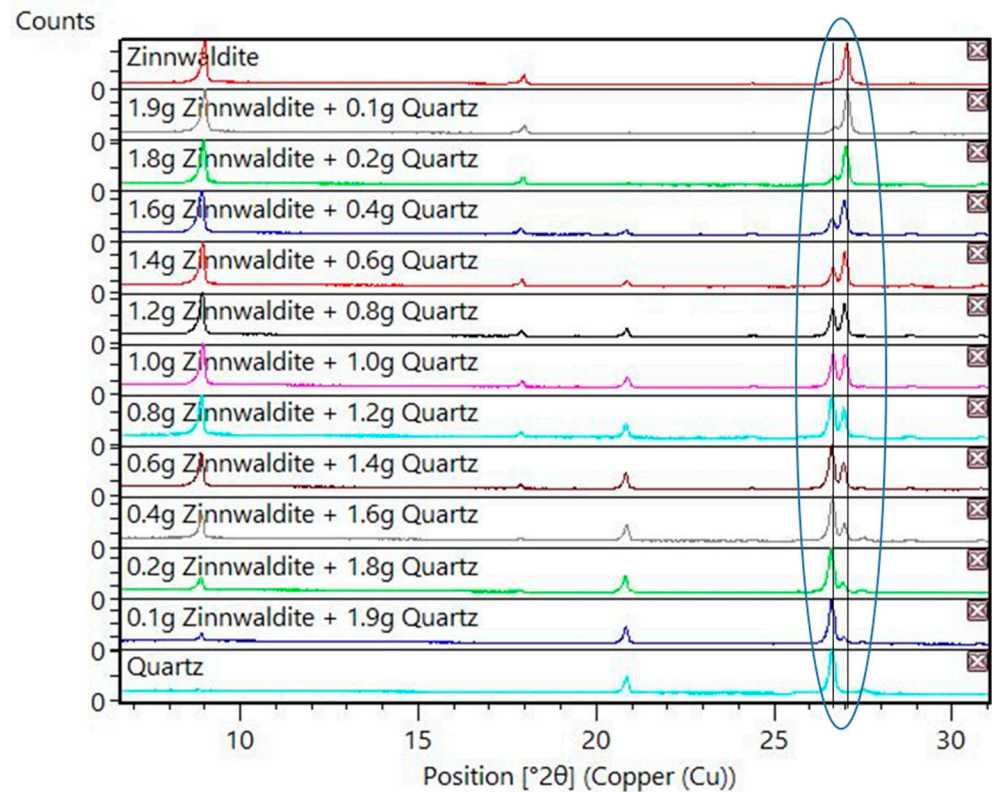


Figure 24. XRD patterns of different zinnwaldite–quartz mixtures with main peaks highlighted.

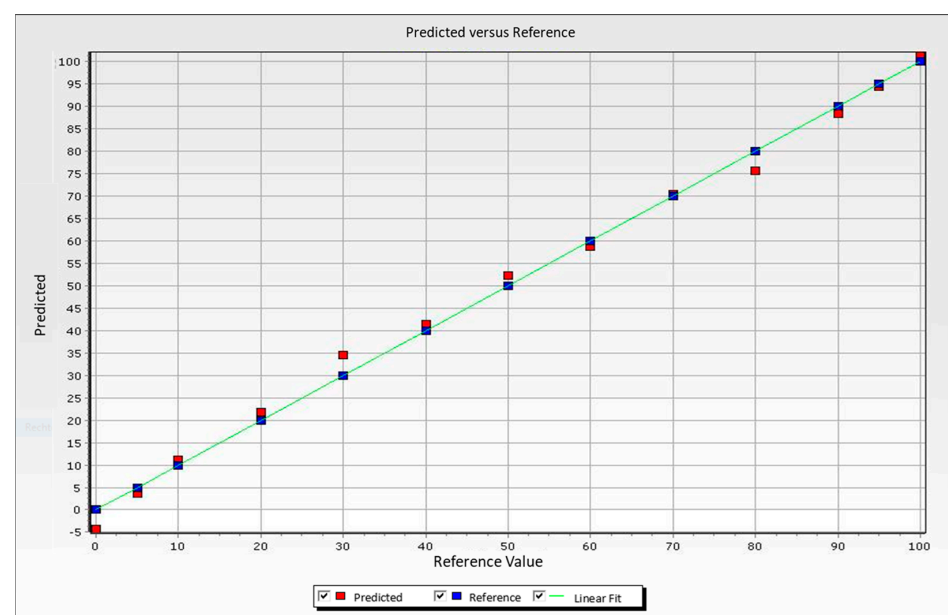


Figure 25. PLSR calibration curve for zinnwaldite–quartz mixtures.

Using the cluster calculation, the following four clusters containing different lithium contents based on zinnwaldite can be generated (Figure 26).

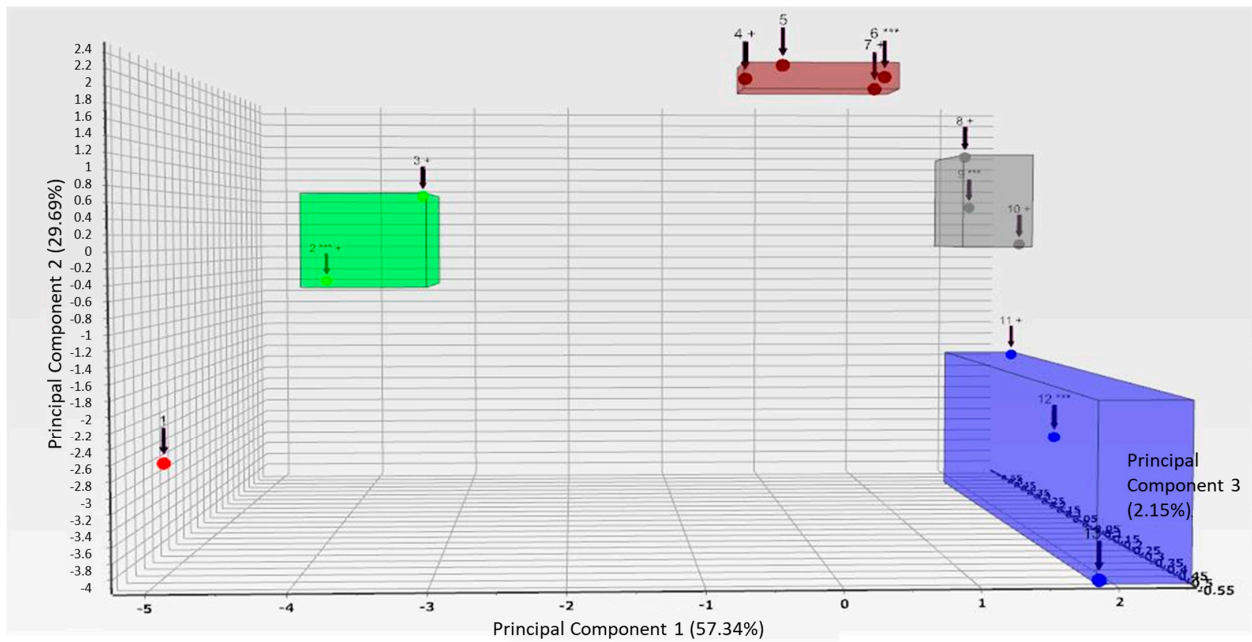


Figure 26. Clusters derived from different zinnwaldite–quartz mixtures. *** most representative sample of cluster, + are the most different ones in the clusters.

The XRD patterns used for PLSR calculation and the different XRDs in the clusters are given in Figure 27.

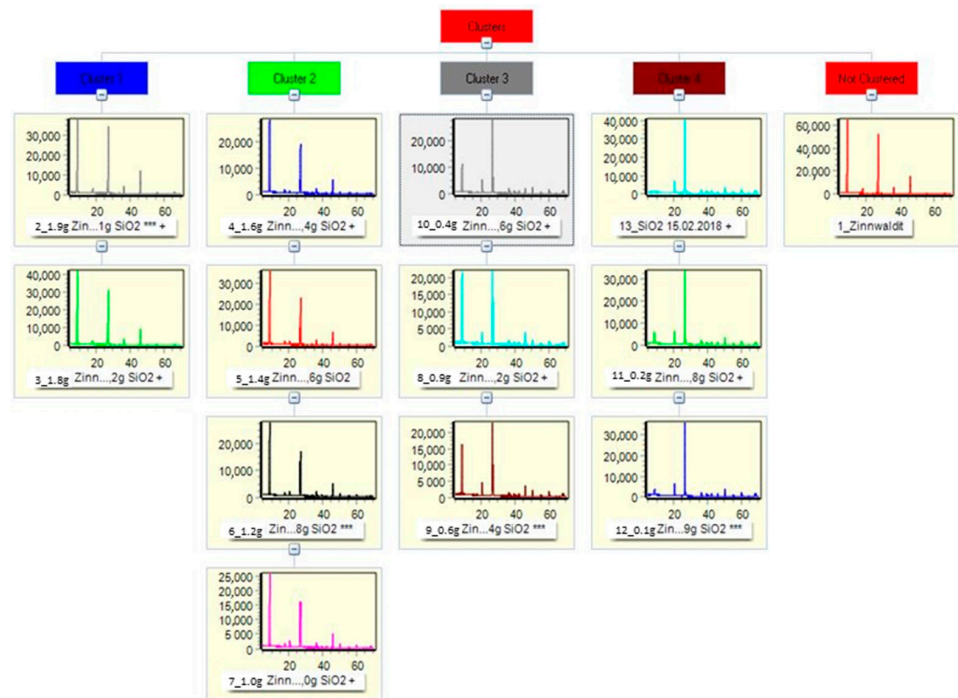


Figure 27. XRD patterns of the different cluster in zinnwaldite–quartz mixtures.

3.7. Analysis of Complex Lithium Ores and Process Mixtures

Different compositions of complex ores from different parts of the world were also analyzed and compared (Figure 28). These mixtures were all put into separate clusters by cluster analysis due to their mineralogical variances.

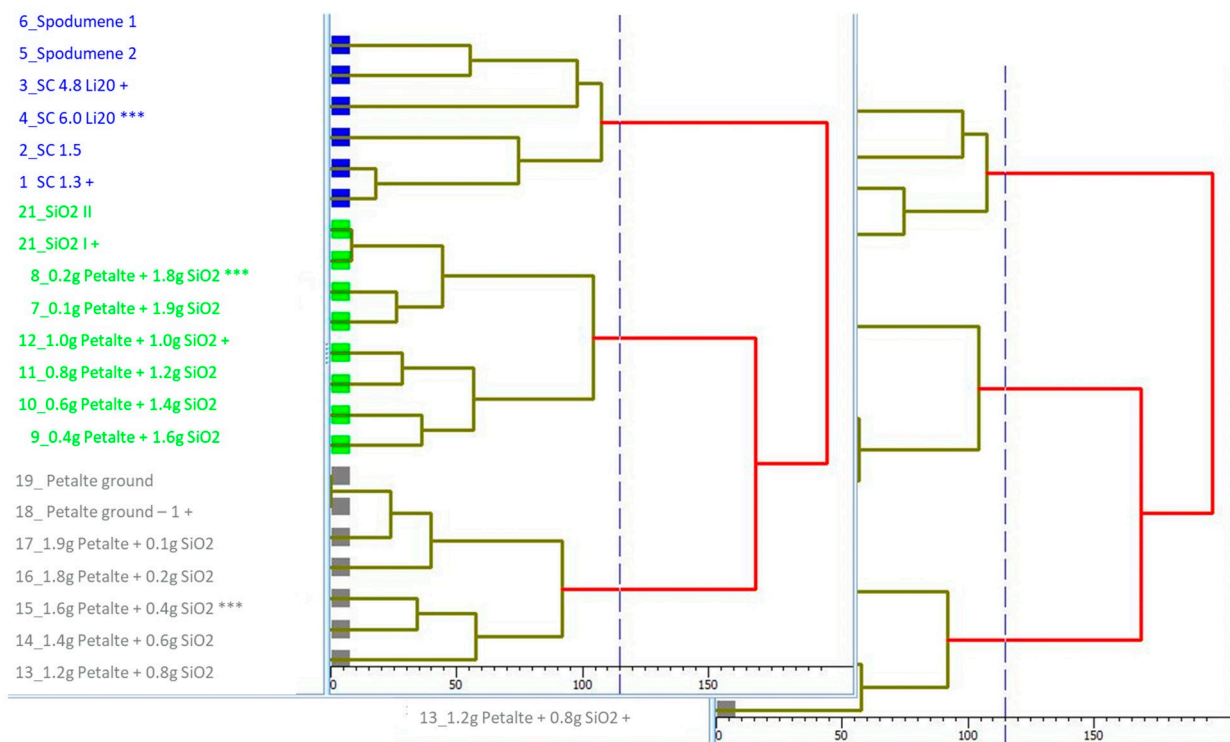


Figure 28. Dendrogram showing lithium ores from different parts of the world arranged in different clusters.

Some more ores from different parts of the world were clustered into lithium-rich mineral ores and those having higher contents of quartz. The different main lithium minerals which composed these ores could also be clustered. The different lithium ore minerals were arranged in different clusters due to their varying XRD-patterns, representing also different Li_2O -contents. A separation of the different lithium ores to different mines is possible. As the mica minerals zinnwaldite and lepidolite show close related and similar XRD patterns and therefore their main peaks do fall in the same cluster areas (Figure 29). In geological surroundings of these lithium ores normally only one type of mica is present and can then be shown, included and clustered separately here.

The following five lithium containing clusters could be separated Cluster 1: MICA: lepidolite–zinnwaldite, Cluster 2: triphylite, Cluster 3: petalite, Cluster 4: amblygonite, and Cluster 5: spodumene (Figure 29).

3.8. Investigation of Complex Ores Composed of Spodumene, Mica (Lepidolite), Quartz and Feldspar

Different binary, ternary, and quaternary mixtures in relevant compositional mineralogical variances from different occurrences were investigated. In Figure 29, the different mixtures are shown to fall into separate clusters from mixtures containing different minerals. The clusters represent XRD patterns with high contents of the lithium minerals, but also some with ternary mixtures including gangue minerals (spodumene, quartz and mica). The combinations of binary mixtures of quartz-spodumene, quartz-feldspar and feldspar-spodumene out of the quaternary tetrahedron including mica is given in Figure 30, represented by their PLSR calibration curves.

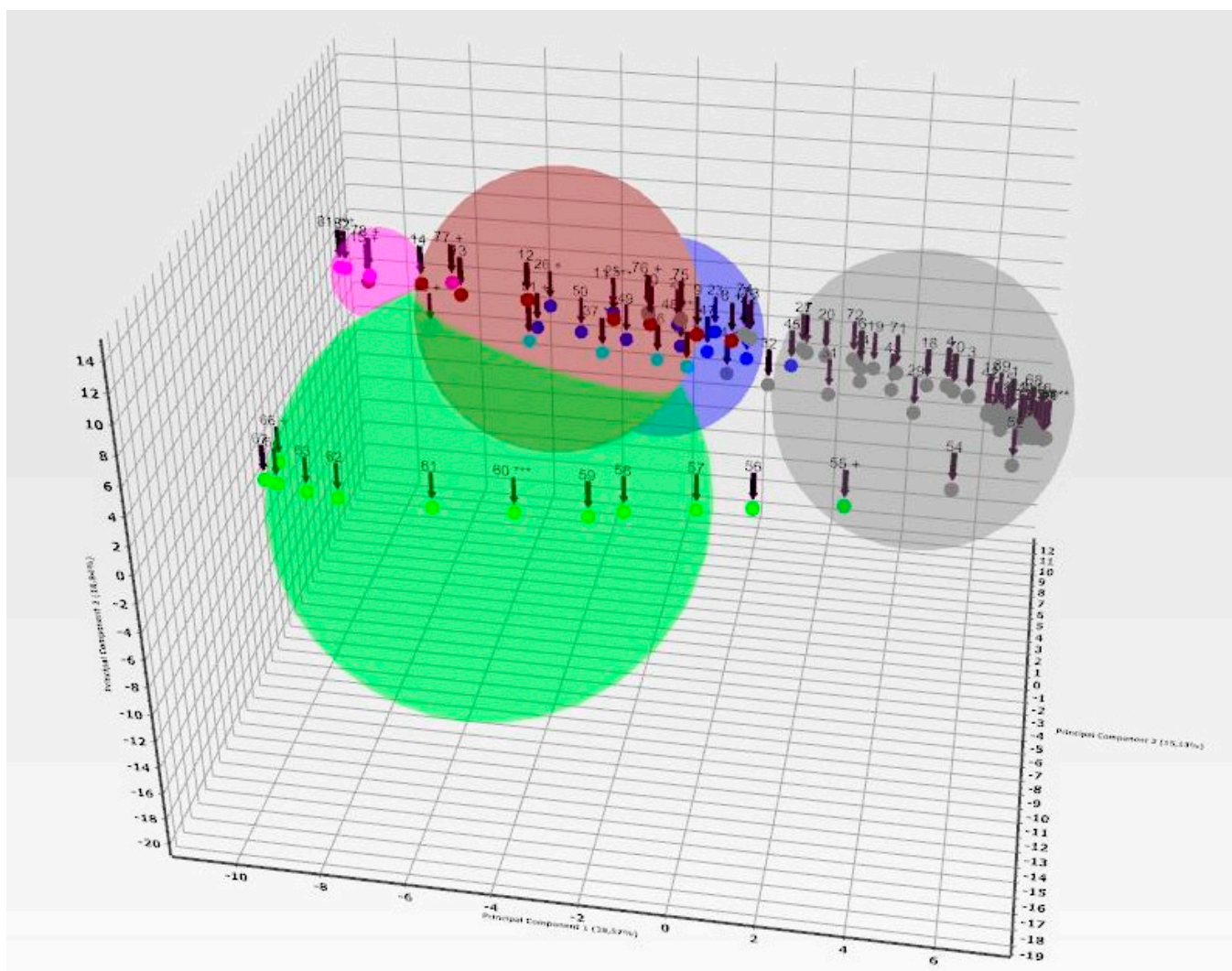


Figure 29. Five Clusters of different lithium mineral ores from different parts of the world with the main minerals separated into different clusters. *** most representative XRD, + most different XRD's in the cluster.

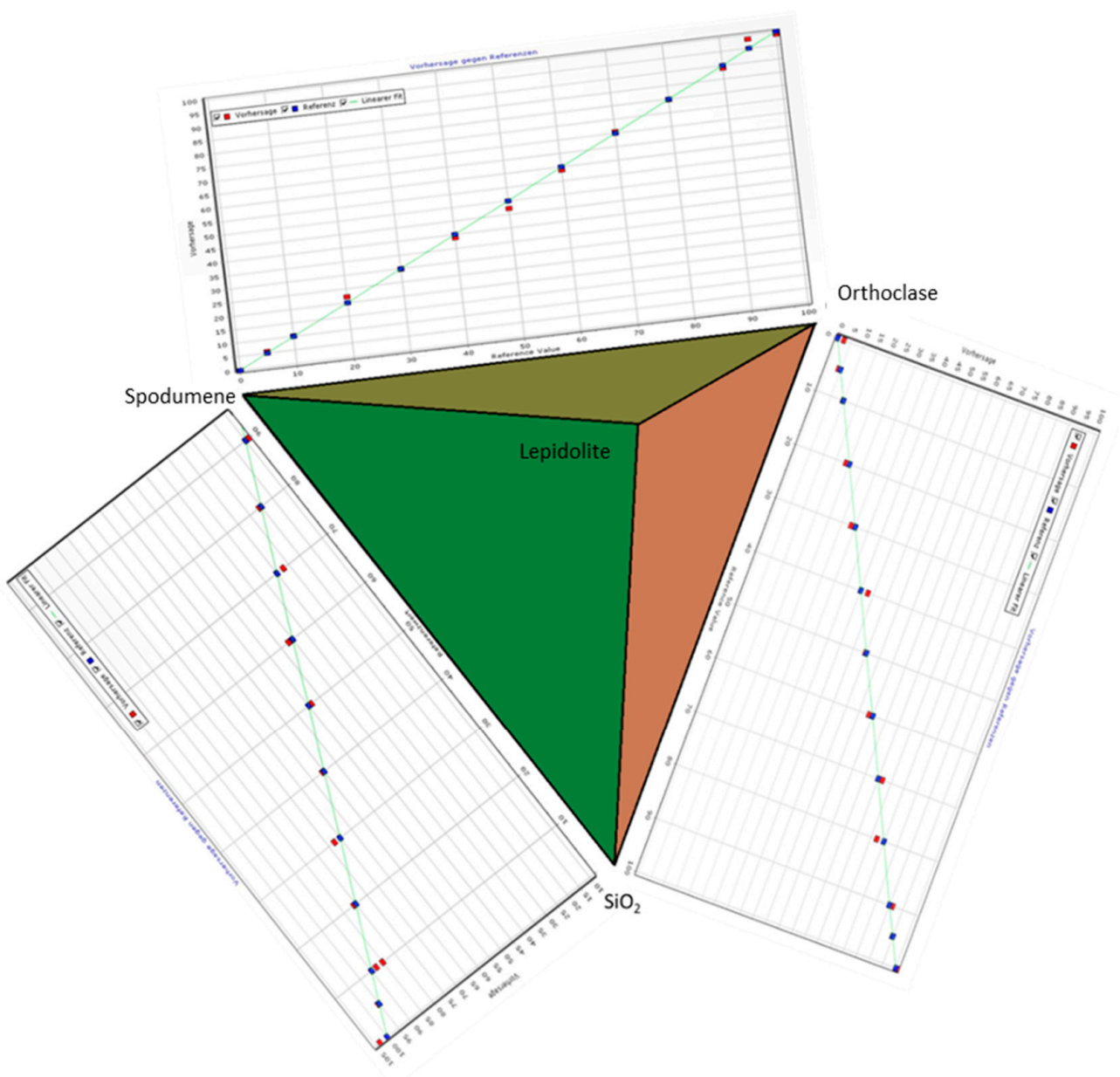


Figure 30. Calibration curves of the three binary mixtures in the system quartz-feldspar-spodumene arranged along the triangle spodumene-quartz-orthoclase.

It is also possible to treat complex mixtures by XRD, using statistical methods. The three calibration curves for binary mixtures obtained by PLSR techniques are given in Figure 30. The binary and ternary calibration curves including orthoclase, spodumene and quartz are given in Figure 31a–c. For ternary mixtures the calibration curves can be derived also by PLSR (Figure 31d) and are based on increasing spodumene contents. In Figure 32 the derived 4 clusters of the different mineral mixtures (binary and ternary) are given.

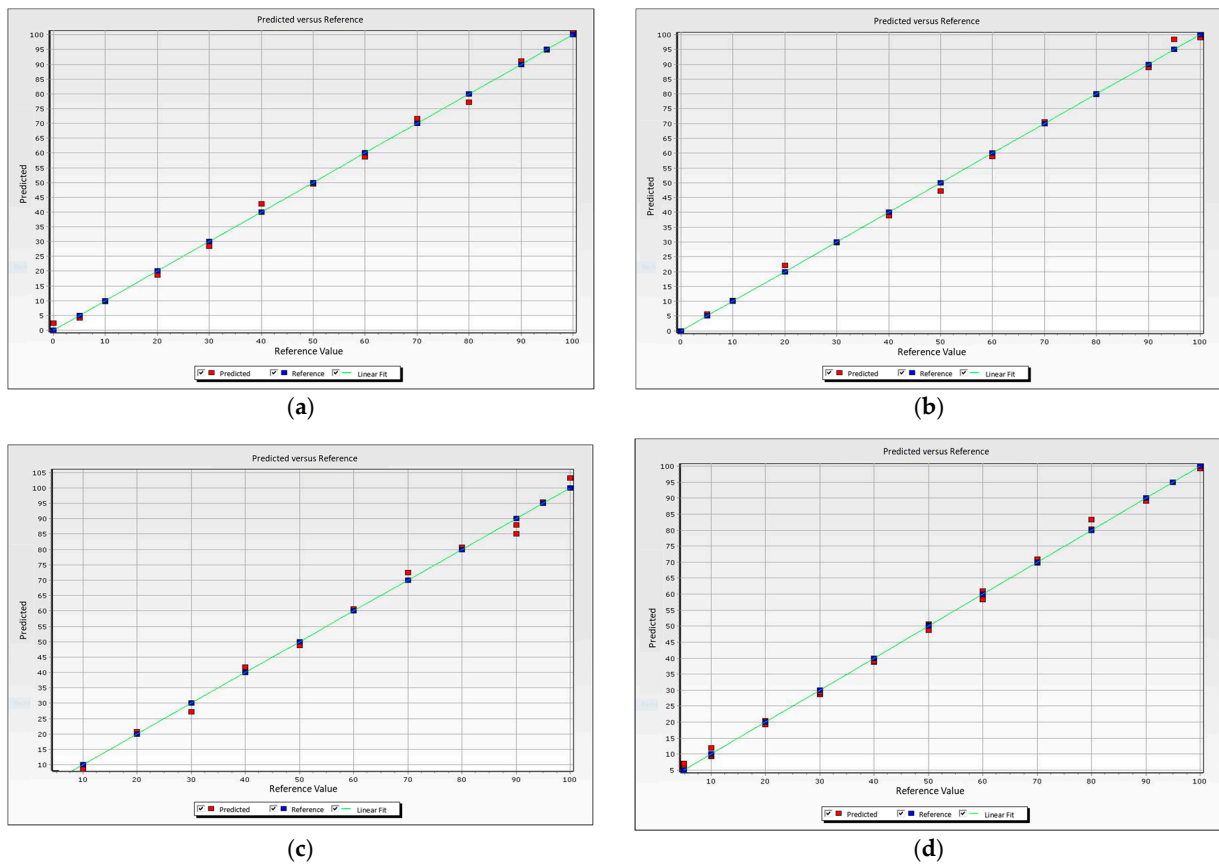


Figure 31. (a) Calibration curve of binary system orthoclase–quartz, (b) calibration curve of binary system orthoclase–spodumene, (c) calibration curve of binary system spodumene–quartz, and (d) calibration curve for spodumene in ternary mixtures orthoclase–spodumene–quartz.

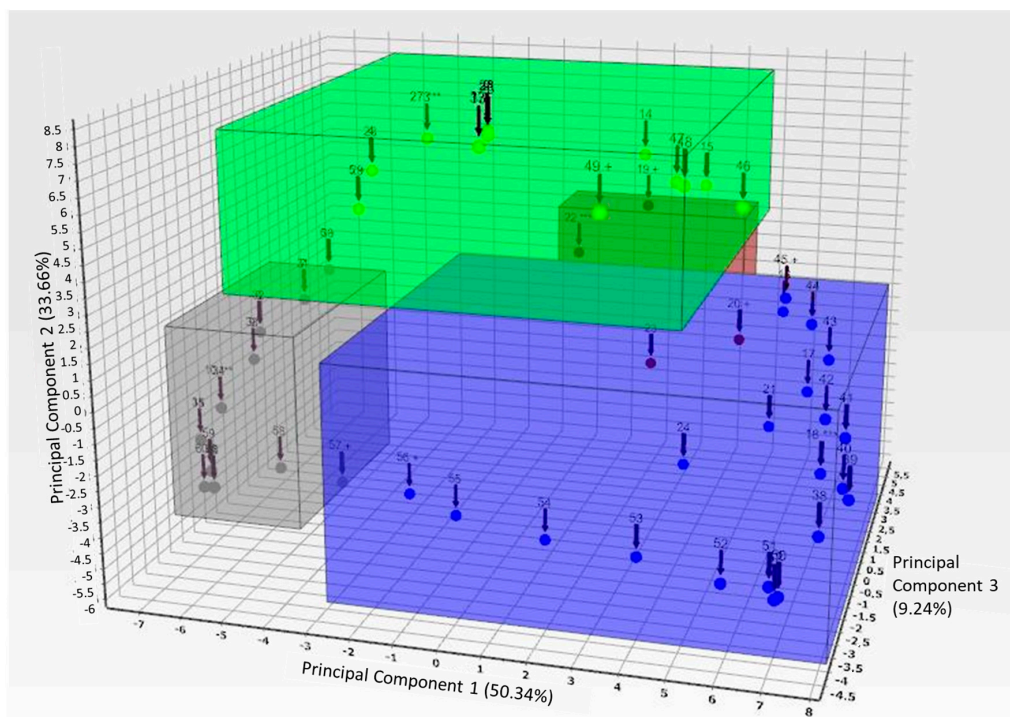


Figure 32. Separate clusters of three binary and one ternary mixture of minerals orthoclase, quartz, and spodumene.

In Figure 32 the four clusters of spodumene-rich, quartz-rich, orthoclase-rich, and ternary mixtures can be calculated.

When this system is opened up by the addition of all of the other already described binary mixtures containing lithium minerals, the clusters containing different, but definite mineral associations can be derived as given in Figure 32. These arrangements are basically due to the relevant lithium-containing mineral from which the Li_2O content can be calculated.

By the aid of this technique the different mineral associations can be separated and different mixtures of lithium containing minerals are separated (Figure 33). Only lepidolite and zinnwaldite, due to their similar XRD patterns (typical mica XRD patterns), are difficult to distinguish from each other. In practical measurements from different occurrences worldwide, not all these different combinations will be available, which concludes that these calculations for lithium minerals are even more simple to obtain.

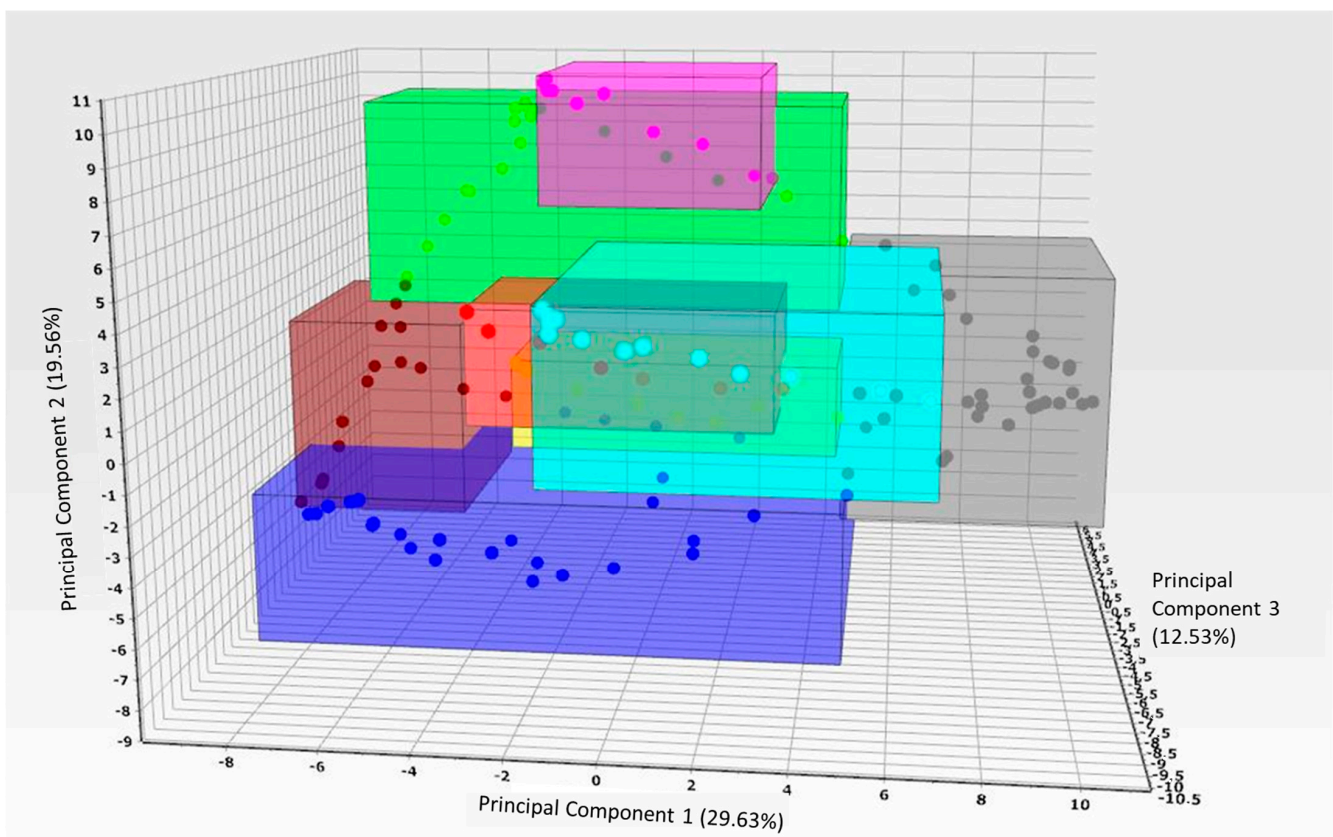


Figure 33. PCA analysis of binary, ternary, and quaternary mixtures containing all six different lithium minerals, and orthoclase and quartz, one cluster is formed containing two mica minerals.

A definite content of lithium oxide can be derived from all these mixtures, making a wet chemical analysis of lithium redundant.

4. Investigation of Special Hard Rock Ores and Brines—Industrial Case Studies on Complex Ores

4.1. Hard Rock Lithium Deposits—Characterization of Raw and Processed Materials

Lithium hard-rock ores are extracted either using open-pit or underground mining. The economically valuable fraction of lithium hard rock deposits is represented by spodumene, apatite, lepidolite, tourmaline, and amblygonite, of which spodumene is the most common lithium-bearing mineral. The gangue fraction of lithium hard-rock deposits typically consists of quartz, feldspar and other silicates.

Figure 34 describes the basic steps to extract lithium carbonate from pegmatite hard rock deposits. After crushing and separation of non-valuable ore, α -spodumene is concentrated by grinding and flotation. Byproducts such as quartz-feldspar sand can be used as filler material in various applications. α -Spodumene is calcined into β -spodumene to enable further processing towards lithium carbonate or hydroxide. Leaching, dewatering, removal of impurities, crystallization, and filtration transform β -spodumene into lithium carbonate or hydroxide. The byproduct analcime, a porous zeolite, can be used in several applications during manufacturing of ceramics, cement, and asphalt.

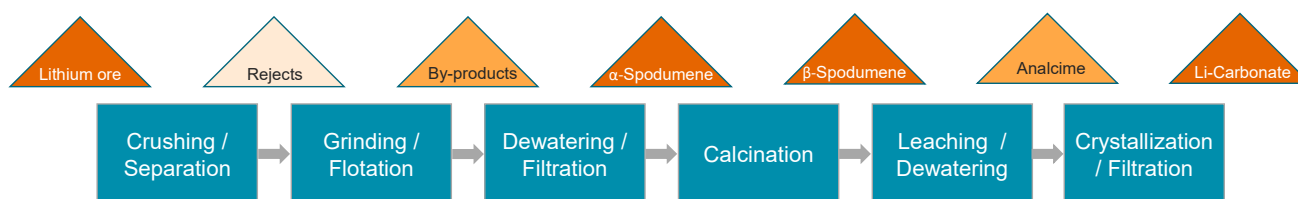


Figure 34. Schematic flow sheet for production of lithium carbonate from hard rock deposits.

The different minerals of hard rock lithium ores have different properties during processing and influence the efficiency of flotation and calcination. Therefore, frequent mineralogical monitoring allows to sort and blend different ore grades to ensure a consistent quality for processing, minimize costs for reagents and reach optimal recovery rates.

Fourteen samples including raw ores as well as processed material (flotation and calcination) were mineralogically analyzed for this case study. A benchtop X-ray diffractometer Aeris Minerals was used for the case study. Five minutes of measurement time per samples was chosen to enable fast and frequent monitoring in a process environment [15].

Prior to phase identification and quantification, cluster analysis of the raw ore samples ($n = 9$) was trialed to investigate the potential of fast ore sorting based on mineralogical information from XRD measurements. Two cluster (groups of similar samples) could be identified as well as two outliers (not belonging to any cluster), (Figure 35). Later mineral quantification will show, that these two clusters reflect high- and low-grade ores and can potentially be used to identify different ore domains in the mine.

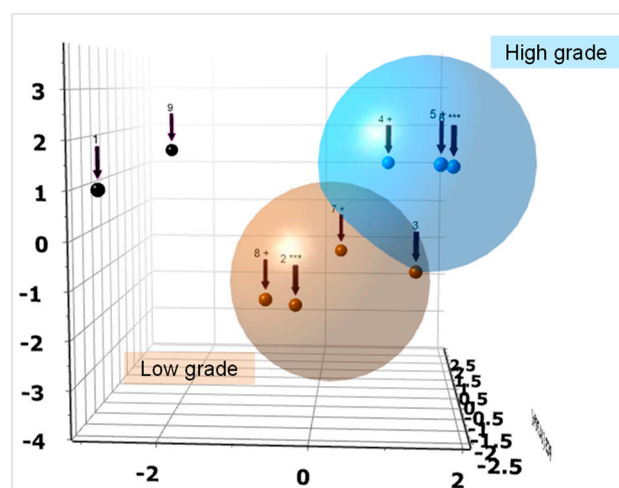


Figure 35. PCA (principal component analysis) plot with two different cluster of lithium ores representing different ore grades ($n = 9$), *** indicates the most representative scan of a cluster, + indicates the two most different scans within one cluster.

Figure 36 shows the XRD patterns of the representative raw ore sample, α - and β -spodumene concentrates and corresponding tailings.

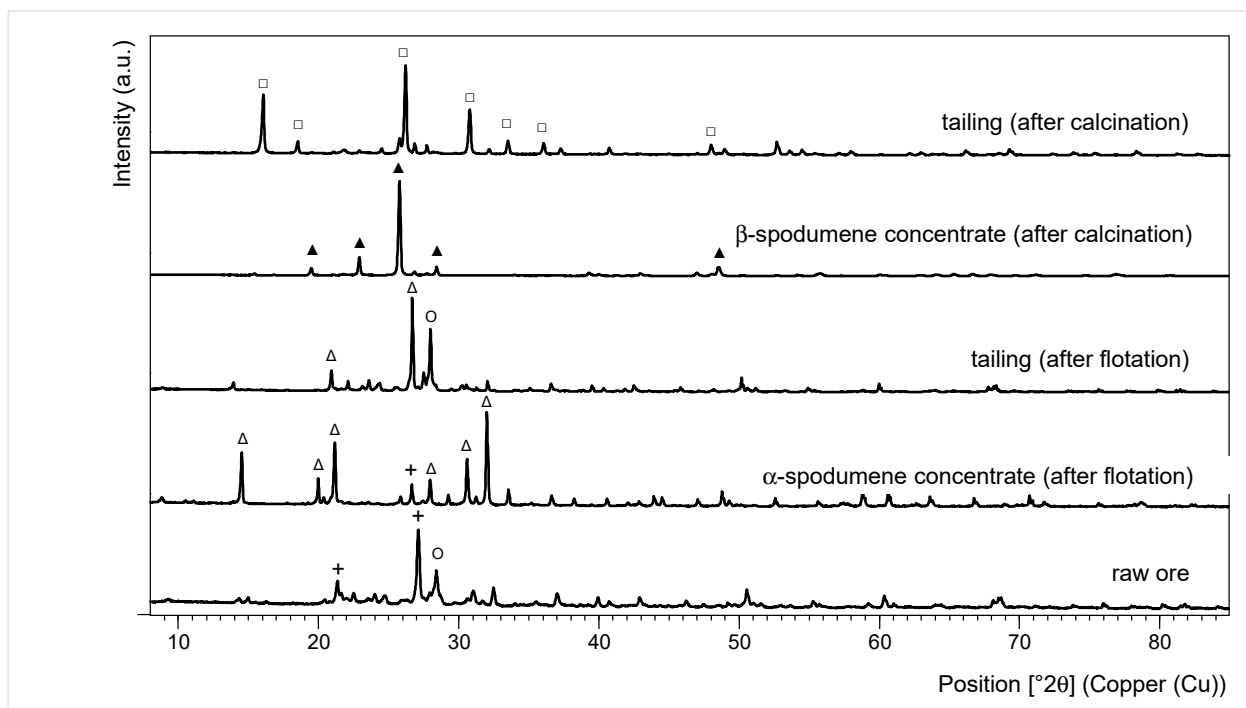


Figure 36. XRD patterns from lithium ore, concentrates and tailing after flotation and calcination, Δ — α -spodumene, \blacktriangle — β -spodumene, O —albite, $+$ —quartz, \square —analcime, modified after Norberg et al. (2020) [37].

Phase identification of the ore samples revealed a complex mineralogy. Main minerals identified are spodumene $\text{LiAl}(\text{SiO}_3)_2$, quartz SiO_2 , albite $\text{NaAlSi}_3\text{O}_8$, anorthite $\text{CaAl}_2\text{Si}_2\text{O}_8$, minor amounts of lepidolite $\text{K}(\text{Li},\text{Al})_3(\text{Al},\text{Si},\text{Rb})_4\text{O}_{10}(\text{F},\text{OH})_2$, orthoclase KAlSi_3O_8 and traces of tourmaline (elbaitite) $\text{Na}(\text{Li}_{1.5}\text{Al}_{1.5})\text{Al}_6\text{Si}_6\text{O}_{18}(\text{BO}_3)_3(\text{OH})_4$, and beryl $\text{Be}_3\text{Al}_2(\text{SiO}_4)_6$. The major peaks of the main phases are marked in the Figure 36.

The Rietveld method was applied to quantify the mineral concentration of the lithium ore samples. Figure 37 shows an example of the resulting full-pattern Rietveld refinement of one ore sample and relative quantities of all available ore samples. The information about the different ratios of spodumene and gangue minerals can be used to define grade blocks in the mine and to sort and blend ores from different mineralogical domains. Further, ore mineralogy directly influences the efficiency of the flotation step and subsequently spodumene recovery rates. The types and quantities of reagents used during flotation require carefully adjustment based on the mineralogy. In addition, the presence and amount of hard minerals such as quartz allows to react on changing ore composition and enables fast feedback times to ensure optimal lifetime of processing equipment like grinding mills.

Besides the definition of ore grades, XRD can also be used to directly monitor the efficiency during downstream processing. Figure 38 shows the quantitative phase composition of α -spodumene concentrate, tailings, or rejects after flotation [44], the calcined product, and the by-product analcime. For this example, the flotation product contains 89.6% α -spodumene with the minor amounts of quartz, albite, anorthite, and traces of lepidolite, beryl, orthoclase and mainly analcime in the residue. The main fraction of the gangue minerals is separated in the rejects, which primarily consist of albite, quartz, and anorthite.

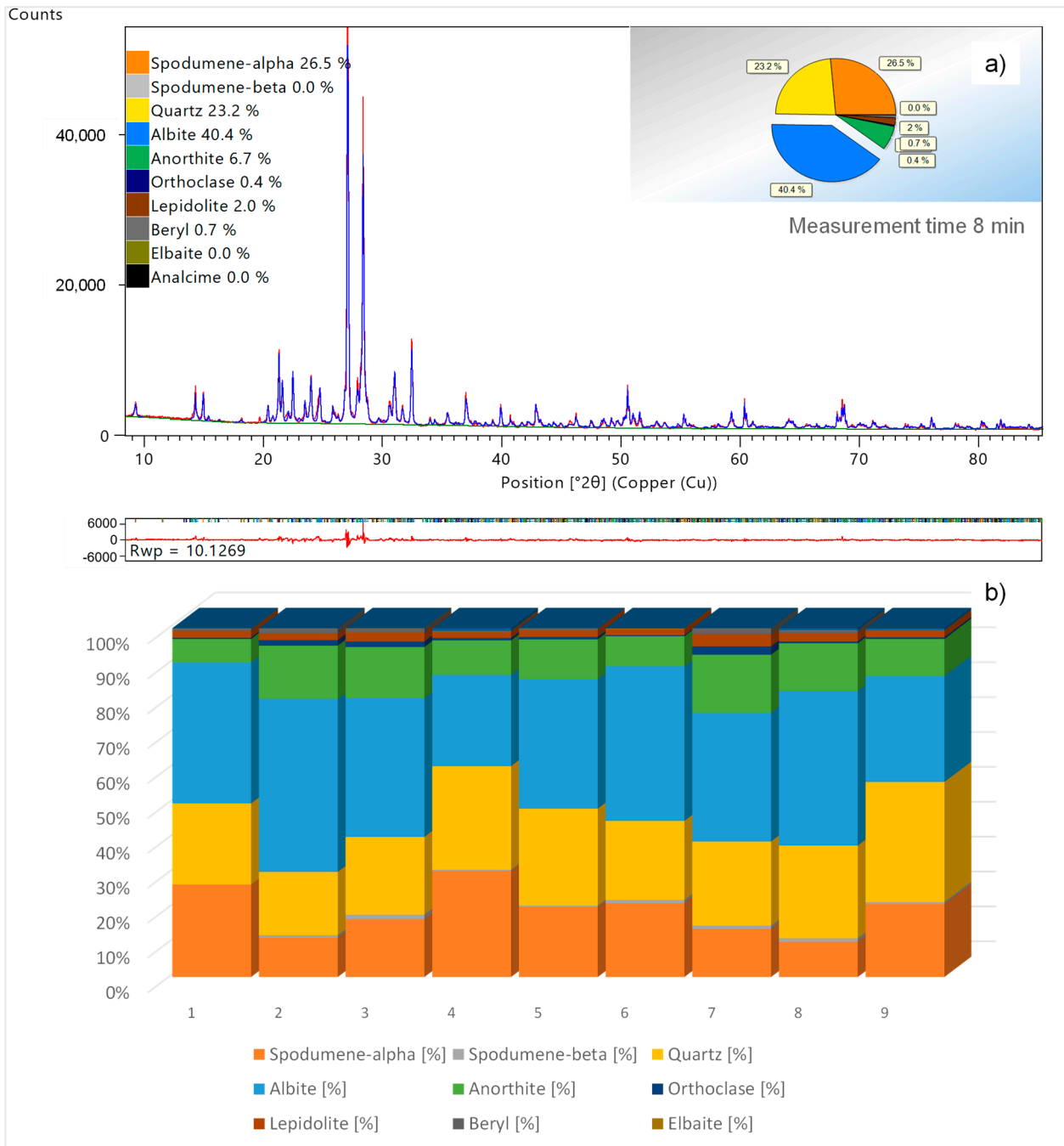


Figure 37. Example of a full-pattern Rietveld quantification of a complex hard-rock lithium ore (a) and variation of mineral quantities in the different products (b).

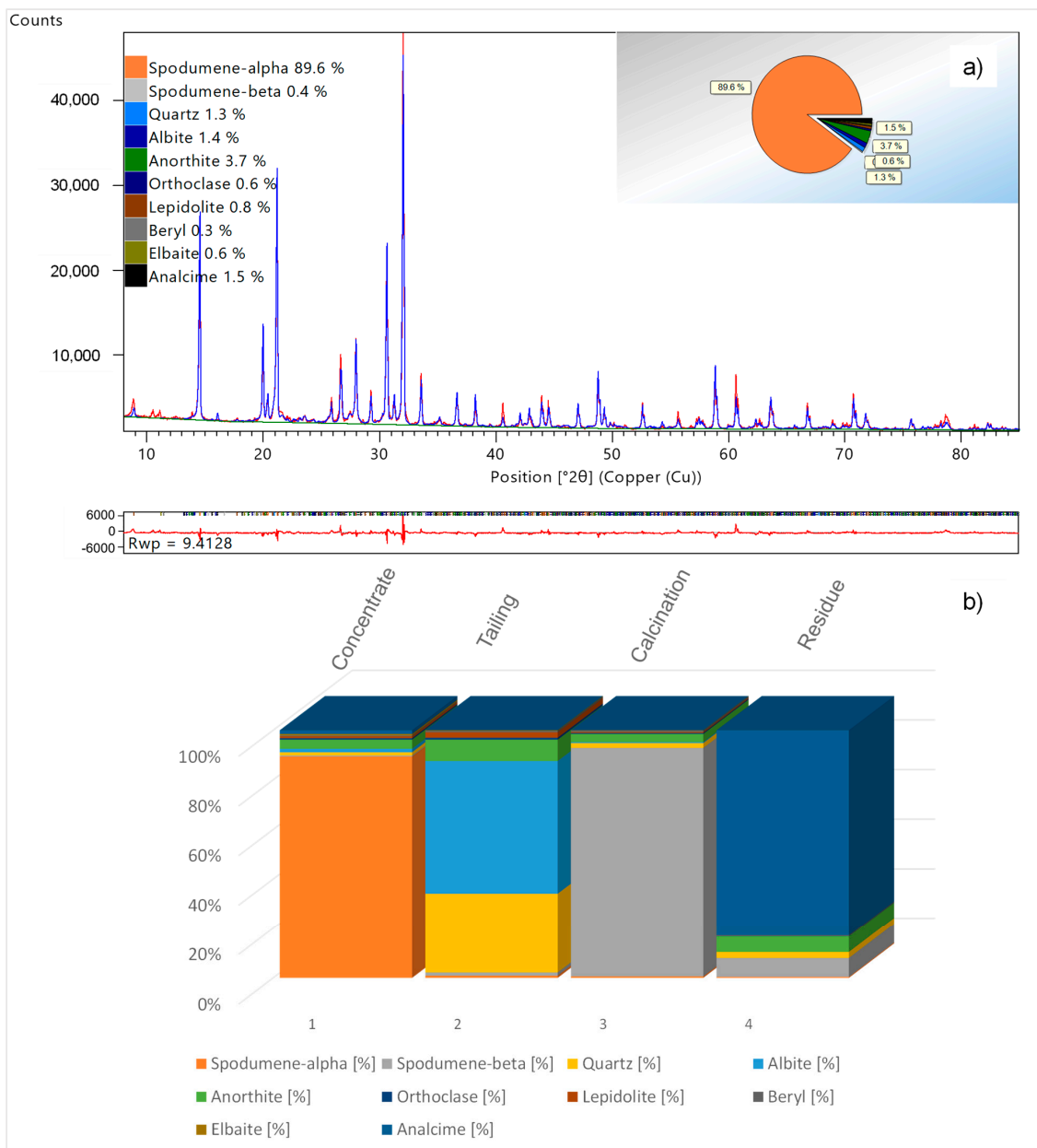


Figure 38. Example of a full-pattern Rietveld quantification of a spodumene concentrate (a) and composition of concentrate, tailing, calcination product and residue (b).

The efficiency of the transformation from α -spodumene to β -spodumene can be monitored by XRD. The two different modifications consist of different crystal structures and show different XRD patterns. In the example in Figure 38, over 92% of the calcined concentrate is transformed into β -spodumene. Impurities are minor amounts of anorthite and quartz. The corresponding by-product analcime still has a residue of β -spodumene that might require adjustments during the calcination process to further increase recovery rates. To summarize the use of XRD for monitoring hard rock lithium ores and processing materials enables easy and fast definition of mineralogical domains in the mine. Cluster analysis can be used as a tool to distinguish fast and easy between different ore grades and allows the definition of grade blocks (Figure 39) and the sorting and blending of ores based on the mineralogical composition. XRD also enables process control during the extraction of β -spodumene from the ore feed.

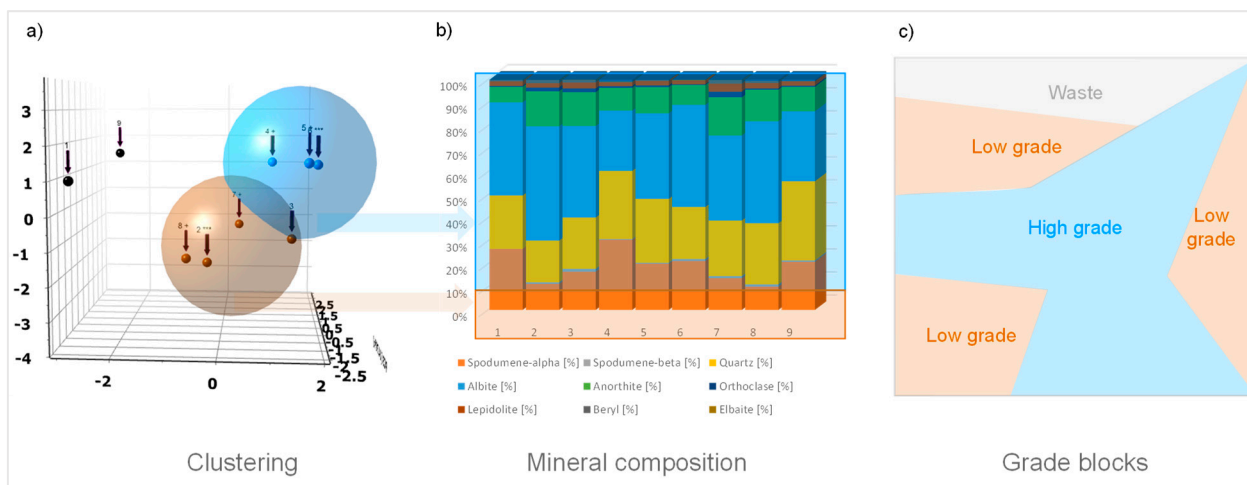


Figure 39. XRD cluster analysis (a), corresponding mineral quantities (b) and visualization of a theoretical grade block model (c) and mineralogical domains of a lithium hard rock deposit.

4.2. Lithium Brines—Mineralogical Characterization of Salts

Besides hard rock lithium deposits, lithium brines are also a main primary resource of lithium with 60% of the global identified reserves [46]. Salars, dried salt lakes, hold 78% of the lithium brine reserves. The process to produce lithium from lithium brines revolves around concentrating the brines up to 6% lithium and removing the impurities subsequently (Figure 40). Careful monitoring of the different salts crystallizing out of a brine helps to adjust extraction of the lithium.

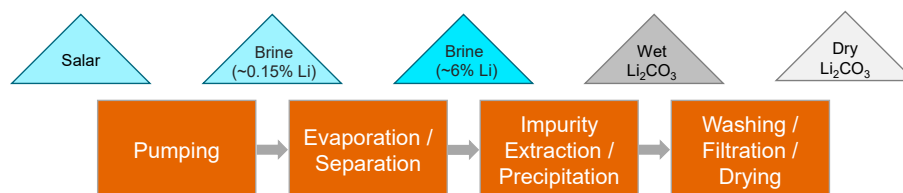


Figure 40. Simplified flow sheet for production of lithium carbonate from brines.

Forty-three samples from a lithium brine were used to cluster, identify and quantify the different mineral phases. Focus of this study was to find a fast way to characterize different salt domains. Due to the hygroscopic behavior of some salt phases, special attention was also put on the optimal sample preparation for the XRD measurements. Lithium salts like Li-Carnallite or Li-Sulfates are hygroscopic under ambient conditions and changing from solid to liquid within minutes. Although XRD offers short measurement times of about 5 min, the hygroscopic behaviour challenges phase identification and quantification. Figure 41 shows the measurement of one sample from a brine containing lithium salts. Extremely short measurement times of 1 min were chosen to follow to decrystallization of Li-Carnallite. Within 10 min all Li-Carnallite peaks disappear completely whereas the other salts are still stable. To avoid decrystallization a capton foil was used on top of the sample during the measurement (Figure 42). After 10 min, Li-Carnallite still appears crystalline and all corresponding peaks have the same intensities.

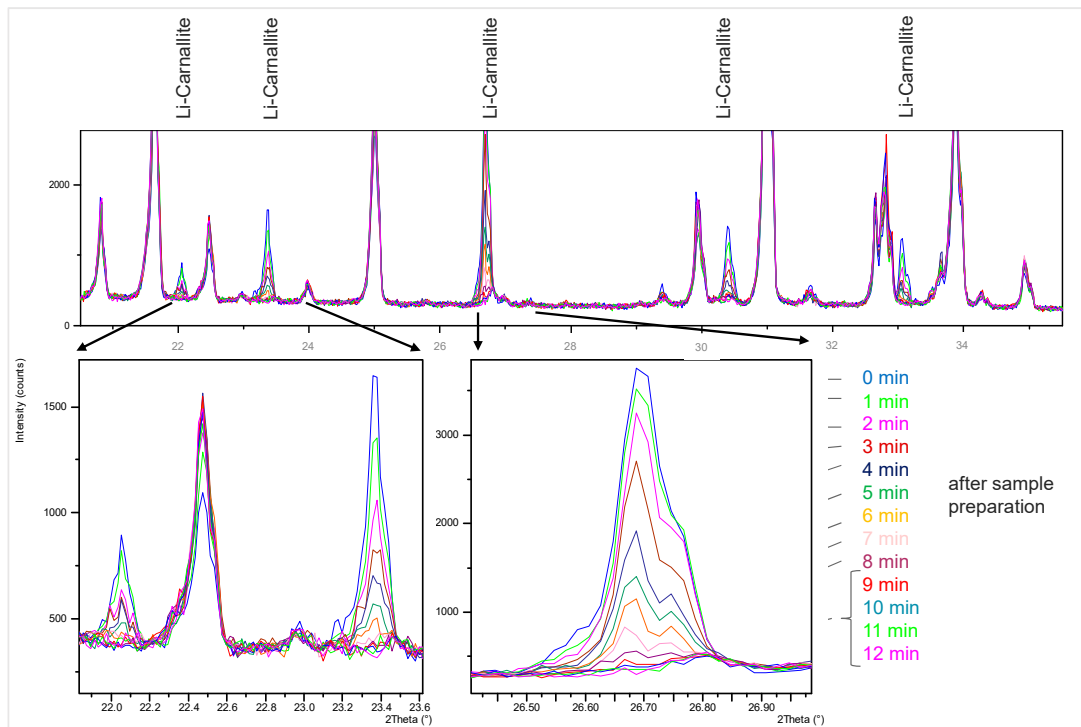


Figure 41. XRD measurement of one brine sample containing lithium carnallite using an open sample holder under ambient conditions, sample measured in 1 min intervals directly after preparation.

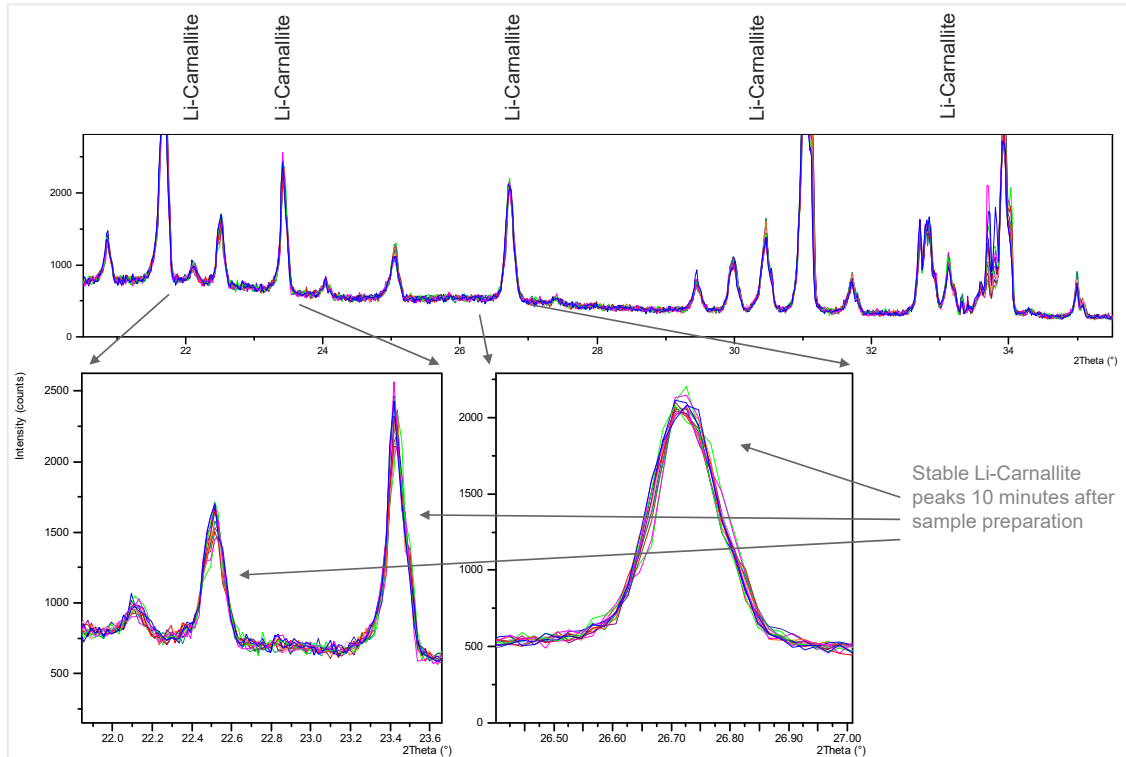


Figure 42. XRD measurement of one brine sample containing lithium carnallite using capton foil on top of the sample, measured in 1 min intervals directly after preparation.

To investigate a fast method to identify and monitor different types of salts with different mineralogical composition, cluster analysis was applied using all 43 available

samples. Figure 43 shows a principal component analysis (PCA) with corresponding dendrogram, identifying seven distinct clusters. During subsequent quantification of all samples the different cluster could be connected to a certain mineral composition. Not only the chlorides, sulfates, and lithium containing salts could be separated, but also samples with different ratios of the minerals (e.g., halite and sylvine).

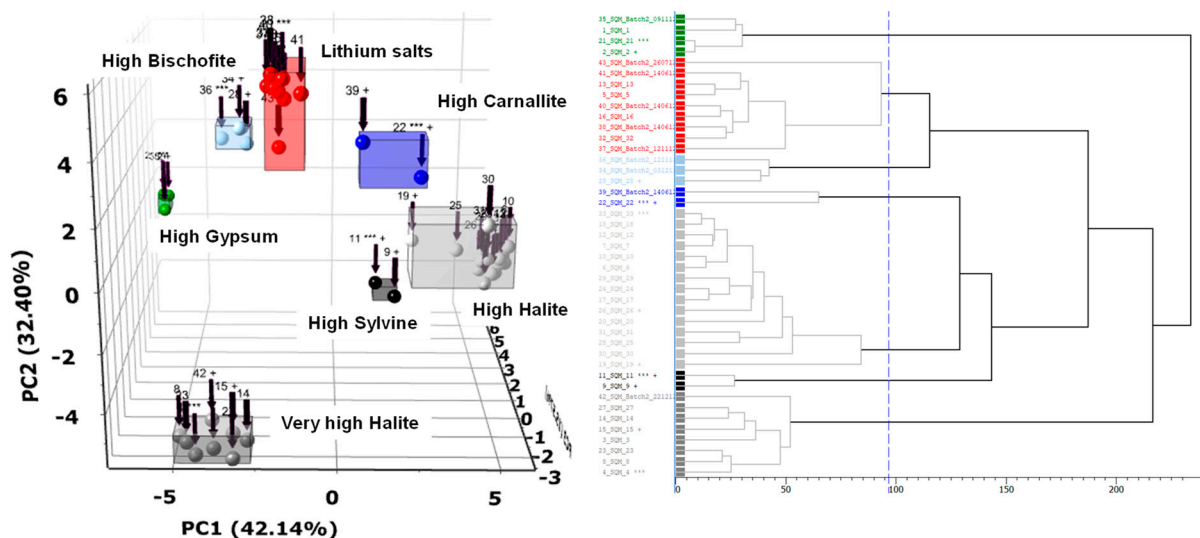


Figure 43. Cluster analysis identifying different clusters of evaporites from a lithium brine deposit ($n=43$) and the relevant dendrogram, *** indicates the most representative scan of a cluster, + indicates the two most different scans within one cluster.

For the set of 43 samples, 13 different mineral phases are identified using XRD, Table 4. Main lithium containing phases are Li-Carnallite and Li-Sulfate Monohydrate.

Table 4. Minerals identifies in the brine samples investigated.

Mineral	Formula
Halite	NaCl
Sylvine	KCl
Carnallite	$KMgCl_3 \cdot 6H_2O$
Bischofite	$MgCl_2 \cdot 6H_2O$
Chloromagnesite	$MgCl_2$
Anhydrite	$CaSO_4$
Gypsum	$CaSO_4 \cdot 2H_2O$
Syngenite	$K_2Ca(SO_4)_2 \cdot H_2O$
Polyhalite	$K_2MgCa_2(SO_4)_4 \cdot 2H_2O$
Kainite	$KMg(Cl,SO_4) \cdot 2.75H_2O$
Picromerite (Schoenite)	$K_2Mg(SO_4)_2 \cdot 6H_2O$
Li-Sulfate Monohydrate	$Li_2SO_4 \cdot H_2O$
Li-Carnallite	$LiMgCl_3 \cdot 7H_2O$

Quantification of the different mineral phases in all samples was applied using the Rietveld method. Figure 44 shows an example of a Rietveld refinement quantifying eight crystalline mineral phases.

The case study demonstrates that XRD can be used to monitor different salts of lithium brines. Special sample preparation is required due to the hygroscopic of the lithium salts. Cluster analysis is a fast method to identify different mineralogical compositions of the salts. Due to measurement times of about 5 min and quantification of the total mineral content (crystalline phases) it is possible to use XRD as process control method to monitor the mining and processing of lithium brines.

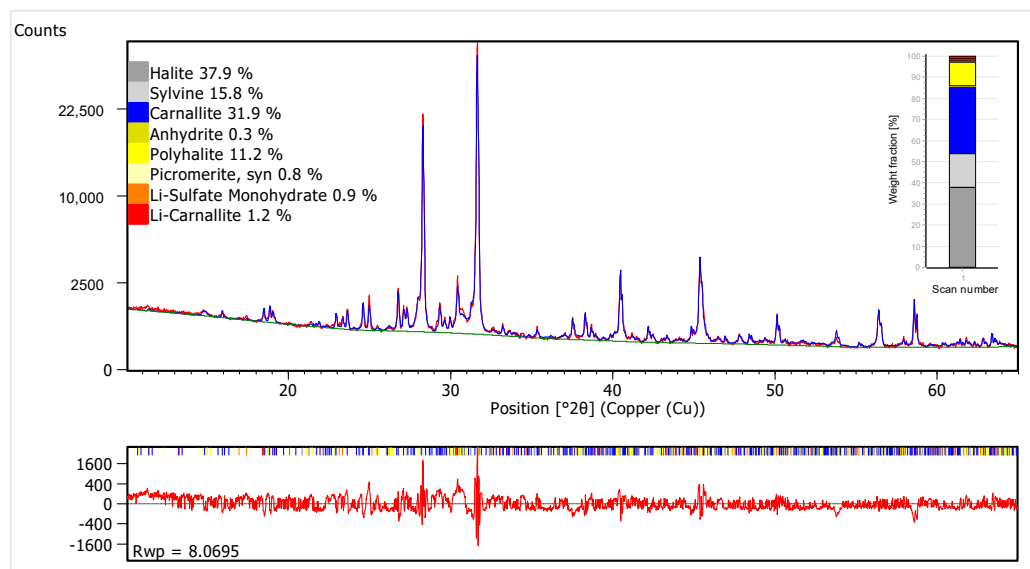


Figure 44. Example of a full-pattern Rietveld quantification of a lithium ore from a brine.

5. Conclusions

By using the XRD method for the quantitative determination of minerals, followed by a recalculation of the Li_2O -content, it is possible to replace the wet chemical analysis and obtain contents of lithium increasingly fast. It could be proved that Li_2O -contents down to 0.1% can be reliably determined in the presented mixtures after definition of the occurring lithium mineral in the sample. The method must be adapted to more complex mixtures. Nowadays besides the determination of lithium in primary ores the determination of lithium in lithium mineral leaching residues can also be of interest. It can be summarized as follows:

1. Quantitative lithium determination by mineral quantification is possible;
2. Definite mineral composition must be known for calculations of contents;
3. Rapid and fast lithium determination in mineral mixtures by XRD is possible;
4. XRD quantification method is easily applied for simple mineralogical compositions of minerals and can replace wet chemical analysis;
5. XRD methods for typical ternary mineral systems can already be successfully applied;
6. XRD methods and interpretations combined with statistical treatment methods can be applied in practical applications:
 - (A) Rietveld quantification—no calibration curve necessary
 - (B) Partial Least Squares—refinement with calibration curves—rapid and reliable for lithium concentrates
 - (C) Clustering of different lithium mineral compositions—identifies different lithium ore qualities
 - (D) Classic lithium content determination using chemical methods—time consuming but useful for referencing
7. More complex ores and brines can be treated by XRD and useful results are obtained methodology is more complicated;
8. Determination of lithium in brines is more complicated due to lower lithium contents and due to complex mineralogy;
9. For detailed mineralogical determinations a more sophisticated Rietveld analysis is useful for multi-mineral mixtures and more detailed results.

6. Summary

Thus, also XRD technique can be used for the determination of lithium in lithium ores as fast, quantitative and reliable method. The detection limits for the different minerals are

summarized in Table 5. In concentrates however, mainly the higher lithium concentrations are of interest for further processing.

Table 5. Detection of lithium in six different lithium-minerals and their detection limits.

Mineral Name	Detection Limit (% of Li ₂ O)	Detection Limit (Mineral Content in %)	Content Li ₂ O in % (Ideal Composition)
Triphylite	0.1%	<1	9.47
Spodumene	0.1%	1–2	8.03
Amblygonite	0.1%	1	7.4
Lepidolite	<0.1%	<1	7.7
Zinnwaldite	0.1%	1	3.42
Petalite	0.1%	1	4.5

The procedures followed in this type of analysis, using primarily the quantitative mineral content and performing a recalculation of the lithium content in these minerals, can be used on the different raw materials. A short description is given schematically in Figure 45.

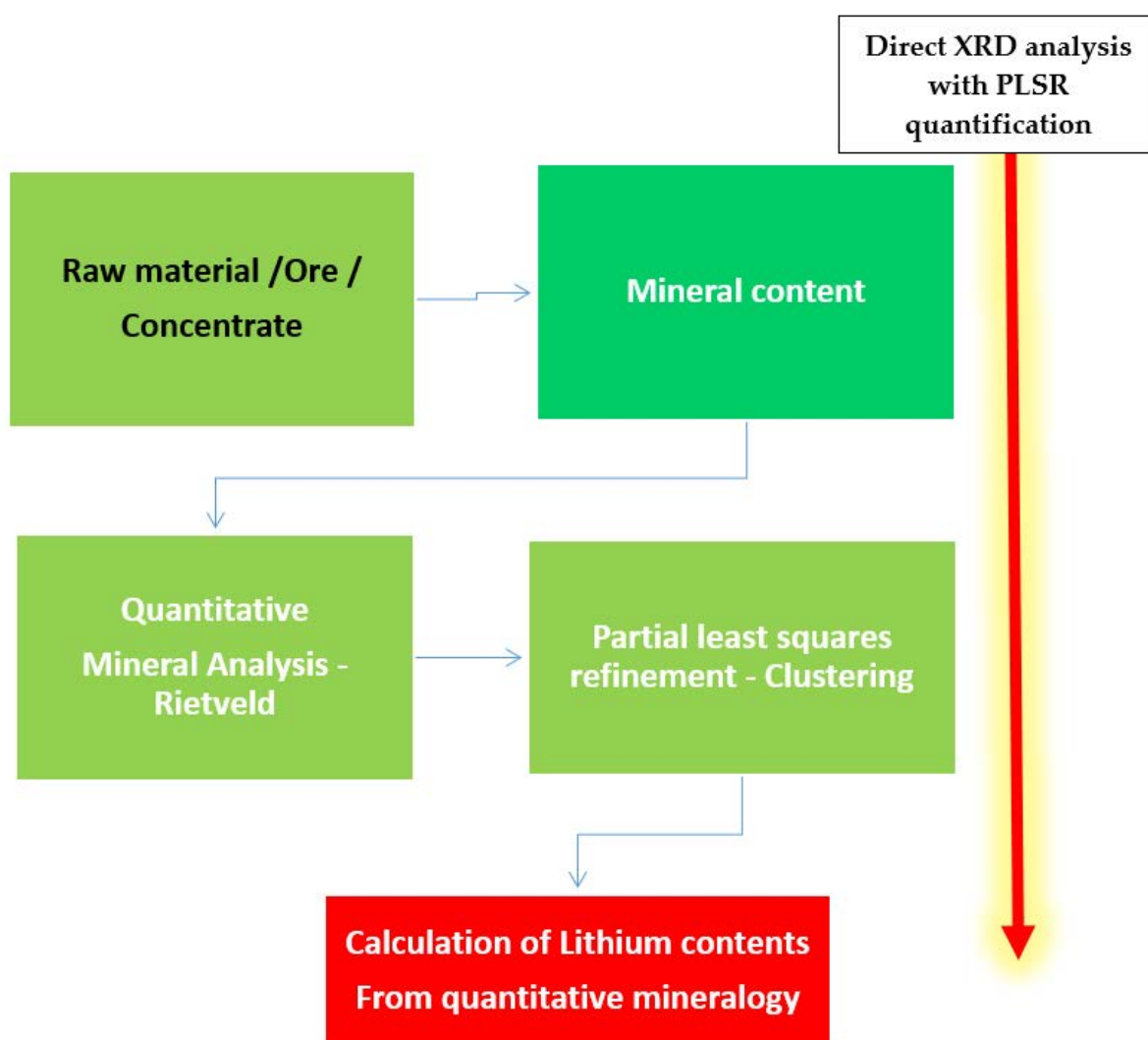


Figure 45. Schematic procedure of lithium determination in lithium ores by XRD.

Some examples of typical concentrates of lithium minerals with quartz were analyzed and their determination results based on the PLSR curves are given in Table 6 and Figure 46. The measured results of different mixtures can be determined rather exactly, sometimes some difference can be observed (maximum 2% of mineral contents). But mainly, very precise contents could be obtained.

Table 6. Examples of PLSR results of lithium ores based on definite initial values given and their measured results from XRD.

Initial Value (%)	Measured Value (%)					
	Spodumene	Triphylite	Petalite	Montebrasite	Zinnwaldite	Lepidolite
10	9.88	8.02	10.34	10.13	10	9.92
50	49.89	50.14	51.32	49.99	49.85	49.93
80	80.02	79.97	80.33	80.02	80.26	79.63
95	95.22	94.75	94.85	95.02	94.93	94.55
97.5			96.1			96.89
99	97.01	97.03				
100					99.7	

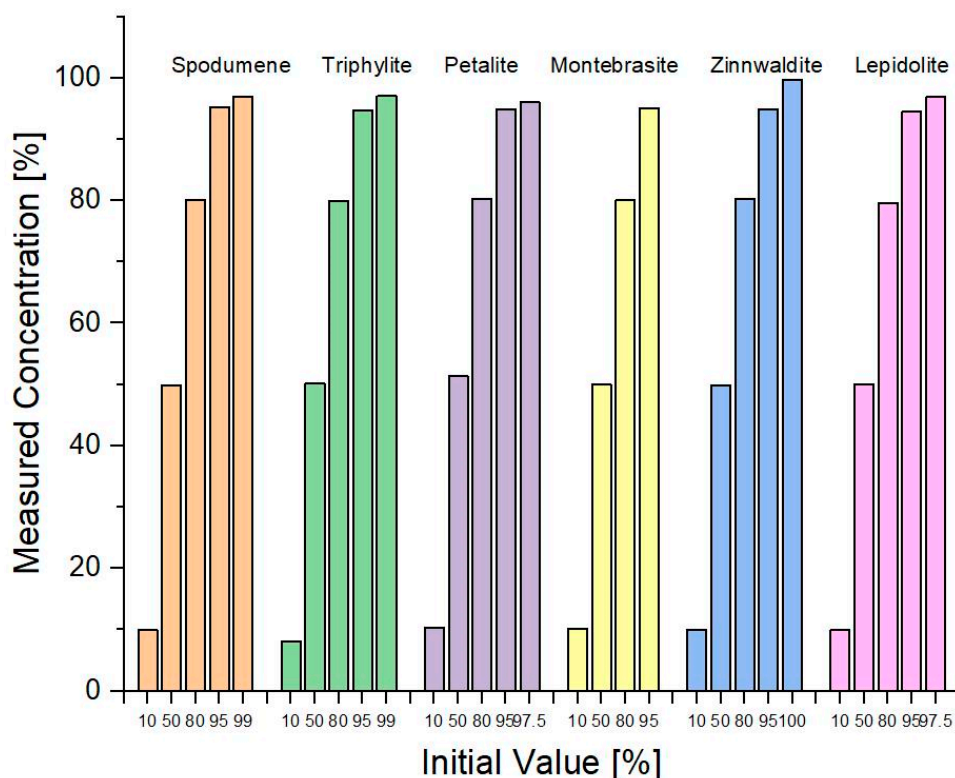


Figure 46. Measurements and results of typical concentrates of the lithium minerals and the measured contents determined by XRD.

Therefore, X-ray powder diffraction (XRD) is an established, fast, and accurate mineralogical method providing valuable information for mining and beneficiation of lithium hard-rock deposits. Accurate mineralogical analysis during mining and processing of lithium ores allows efficient mine planning, ore sorting and blending as well as optimizing the different steps of beneficiation and extraction. XRD is beneficial to optimize the use of expensive reagents in the flotation cells. Mineralogical analysis of concentrates and tailings during flotation and calcination of lithium hard-rock treatment allows fast counteractions on changing ore grades or process conditions and subsequently increases the recovery rate of lithium minerals. Modern diffraction instruments are fast, accurate and compact in size. Their infrastructure can be easily implemented in the process flow at the beneficiation

plant, including full automation, from sampling to results reporting into a centralized plant control system. Compact XRD instruments can even be a part of a mobile container lab, located directly at a mine site. Automated sample preparation in combination with intuitive measurement flow setup and fully automated analysis significantly low is the entry level, required to operate a modern XRD instrument in the efficient manner.

Author Contributions: Conceptualization first part, H.P., second part, U.K.; methodology, H.P. and U.K.; writing and editing done by both authors; investigation done at University of Halle and Panalytical analytical laboratories in Almelo/Netherlands. All authors have read and agreed to the published version of the manuscript.

Funding: This research was not funded externally but resources of University of Halle/mineralogy were used.

Data Availability Statement: All data were gathered and treated at mineralogy laboratories at University of Halle and Panalytical laboratories in Almelo.

Acknowledgments: The financial help by providing analytical instruments at university of Halle and the continuous effort of Frau Kummer in the mineralogical laboratories is gratefully acknowledged.

Conflicts of Interest: The authors declare no conflict of interest.

References

1. Chaussidon, M.; Robert, F. Lithium nucleosynthesis in the Sun inferred from solar wind $7\text{Li}/6\text{Li}$ ratio. *Nature* **1999**, *402*, 270–273. [[CrossRef](#)]
2. Liao, B.; Chen, J. The application of cluster analysis in X-ray diffraction phase analysis. *J. Appl. Cryst.* **1992**, *25*, 336–339. [[CrossRef](#)]
3. Penniston-Dorland, S.; Liu, X.-M.; Rudnick, R.L. Lithium isotope geochemistry. *Rev. Mineral. Geochem.* **2017**, *82*, 165–217. [[CrossRef](#)]
4. Pöllmann, H.; König, U. Determination of Lithium Concentrations in Different Ores Determined by X-ray Diffraction and Statistical. In Proceedings of the International Mineralogical Association IMA 2018 Meeting, Melbourne, Australia, 13–17 August 2018.
5. Tomascak, P.B.; Magna, T.; Dohmen, R. *Advances in Lithium Isotope Geochemistry*; Springer International Publishing: Cham, Switzerland, 2016; p. 195.
6. Bibienne, T.; Magnan, J.-F.; Rupp, A.; Laroche, N. From mine to mind and mobiles: Society's increasing dependence on lithium. *Elements* **2020**, *16*, 265–270. [[CrossRef](#)]
7. Evans, K. Lithium. In *Critical Metals Handbook*; Gunn, G., Ed.; American Geophysical Union: Washington, DC, USA, 2014; pp. 230–260.
8. Tadesse, B.; Makuei, F.; Albijanic, B.; Dyer, L. The beneficiation of lithium minerals from hard rock ores: A review. *Miner. Eng.* **2019**, *131*, 170–184. [[CrossRef](#)]
9. Benson, T.R.; Coble, M.; Rytuba, J.J.; Mahood, G.A. Lithium enrichment in intracontinental rhyolite magmas leads to Li deposits in caldera basins. *Nat. Commun.* **2017**, *8*, 270. [[CrossRef](#)] [[PubMed](#)]
10. Bowell, R.J.; Pogge von Strandmann, P.A.E.; Grew, E.S. Lithium: Less is more. *Elements* **2020**, *16*, 4.
11. Bowell, R.; Lagos, L.; de los Hoyes, C.R.; Declercq, J. Classification and characteristics of natural lithium resources. *Elements* **2020**, *16*, 259–264. [[CrossRef](#)]
12. Garrett, D.E. Their deposits, processing. Use and properties. In *Handbook of Lithium and Natural Calcium Chloride*; Elsevier: Amsterdam, The Netherlands, 2004; p. 476.
13. Kesler, S.E.; Gruber, P.W.; Medina, P.A.; Keoleian, G.A.; Everson, M.P.; Wallington, T.J. Global lithium resources: Relative importance of pegmatite, brine and other deposits. *Ore Geol.* **2012**, *106*, 55–69. [[CrossRef](#)]
14. Gourcerol, B.; Gloaguen, E.; Melleton, J.; Tuduri, J.; Galiegue, X. Re-Assessing the European lithium resource potential—A review of hard-rock resources and metallogeny. *Ore Geol. Rev.* **2019**, *109*, 494–519. [[CrossRef](#)]
15. London, D. *Pegmatites. The Canadian Mineralogist. Special Publication 10*; Mineralogical Association of Canada: Quebec City, QC, Canada, 2008.
16. London, D. Reading pegmatites: Part 3—What lithium minerals say. *Rocks Miner.* **2017**, *92*, 420–425. [[CrossRef](#)]
17. Schmidt, M. *Risikobewertung Lithium*; DERA(Deutsche Rohstoffagentur) Rohstoffinformation: Berlin, Germany, 2017.
18. Grew, E.S. The minerals of lithium. *Elements* **2020**, *16*, 235–240. [[CrossRef](#)]
19. Grew, E.S.; Hystad, G.; Toapanta, M.P.; Eleish, A.; Ostroverkhova, A.; Golden, J.; Hazen, R.M. Lithium mineral evolution and ecology: Comparison with boron and beryllium. *Eur. J. Mineral.* **2019**, *31*, 755–774. [[CrossRef](#)]
20. Černý, P.; Ercit, T.S. The classification of granitic pegmatites revisited. *Can. Mineral.* **2005**, *43*, 2005–2026. [[CrossRef](#)]
21. Černý, P.; London, D.; Novák, M. Granitic pegmatites as reflections of their sources. *Elements* **2012**, *8*, 289–294. [[CrossRef](#)]
22. Rietveld, H.M. A profile refinement method for nuclear and magnetic structures. *J. Appl. Crystallogr.* **1969**, *2*, 65–71. [[CrossRef](#)]

23. Bradley, D.C.; McCauley, A.D.; Stillings, L.M. *Mineral-Deposit Model for Lithium-Cesium-Tantalum Pegmatites*; Scientific Investigations Report; U.S. Geological Survey: Reston, VA, USA, 2017; p. 48.
24. Brand, N.; Brand, C. Detecting the Undetectable: Lithium by Portable XRF—Talk S3 Presentation Big Sky Montana. In Proceedings of the DXC Conference, Big Sky, MT, USA, 31 July–4 August 2017.
25. Bale, M.; May, A. Processing of ores to produce tantalum and lithium. *Miner. Eng.* **1989**, *2*, 299–320. [[CrossRef](#)]
26. Bishimbayeva, G.; Zhumabayeva, D.; Zhandayev, N.; Nalibayeva, A.; Shestakov, K.; Levanovsky, I.; Zhanabayeva, A. Technological improvement, lithium recovery methods from primary resources. *Orient. J. Chem.* **2018**, *34*, 2762–2769. [[CrossRef](#)]
27. Braga, P.; Franca, S.; Neumann, R.; Rodriguez, M.; Rosales, G. Alkaline process for extracting lithium from Spodumene. In Proceedings of the 11th International Seminar on Process Hydrometallurgy-Hydroprocess, Santiago, Chile, 19–21 June 2019; pp. 1–9.
28. Choubey, P.K.; Kim, M.-S.; Srivastava, R.R.; Lee, J.-C.; Lee, J.-Y. Advance review on the exploitation of the prominent energy-storage element: Lithium. Part I: From mineral and brine resources. *Miner. Eng.* **2016**, *89*, 119–137. [[CrossRef](#)]
29. Dessemond, C.; Soucy, G.; Harvey, J.-P.; Ouzilleau, P. Phase transitions in the α - γ - β spodumene thermodynamic system and impact of γ -spodumene on the efficiency of lithium extraction by acid leaching. *Minerals* **2020**, *10*, 519. [[CrossRef](#)]
30. Yan, Q.; Li, X.; Yin, Z.; Wang, Z.; Guo, H.; Peng, W.; Hu, Q. A novel process for extracting lithium from lepidolite. *Hydrometallurgy* **2012**, *121–124*, 54–59. [[CrossRef](#)]
31. Shankleman, J.; Biesheuvel, T.; Ryan, J.; Merrill, D. We're Going to Need More Lithium. Bloomberg Businessweek, 7 September 2017. Available online: <https://www.bloomberg.com/graphics/2017-lithium-battery-future/> (accessed on 21 July 2021).
32. Dessemond, C.; Lajioe-Leroux, F.; Soucy, G.; Laroche, N.; Magnan, J.-F. Spodumene—The lithium market, resources and processes. *Minerals* **2019**, *9*, 334. [[CrossRef](#)]
33. Ross, N.L.; Zhao, J.; Sleboznick, C.; Spencer, E.C.; Chakoumakos, B.C. Petalite under pressure: Elastic behavior and phase stability. *Am. Mineral.* **2015**, *100*, 714–721. [[CrossRef](#)]
34. Schneider, A.; Schmidt, H.; Meven, M.; Brendler, E.; Kirchner, J.; Martin, G.; Bertau, M.; Voigt, W. Lithium extraction from the mineral zinnwaldite: Part I: Effect of thermal treatment on properties and structure of zinnwaldite. *Miner. Eng.* **2017**, *111*, 55–67. [[CrossRef](#)]
35. Fehr, K.T.; Hochleitner, R.; Schmidbauer, E.; Schneider, J. Mineralogy, mössbauer spectra and electrical conductivity of triphylite. *Phys. Chem. Miner.* **2007**, *34*, 485–494. [[CrossRef](#)]
36. Norberg, N.; König, U.; Bhaskar, H.; Narygina, O. Accurate mineralogical analysis for efficient lithium ore processing. In Proceedings of the ALTA 2020 Lithium & Battery Technology, Online, 26 November 2020.
37. Rietveld, H.M. Line profiles of neutron powder diffraction peaks for structure refinement. *Acta Crystallogr.* **1967**, *22*, 151–152. [[CrossRef](#)]
38. De Jong, S. SIMPLSR: An alternative approach to partial least squares regression. *Chemom. Intell. Lab. Syst.* **1993**, *18*, 251–263. [[CrossRef](#)]
39. Lohninger, H. *Teach/Me Data Analysis*; Springer: Berlin, Germany; New York, NY, USA; Tokyo, Japan, 1999.
40. Degen, T.; Sadki, M.; Bron, E.; König, U.; Nénert, G. The highscore suite. *Powder Diffr.* **2014**, *29*, S13–S18. [[CrossRef](#)]
41. Kelley, L.A.; Gardner, S.P.; Sutcliffe, M.J. An automated approach for clustering an ensemble of NMR-derived protein structures into conformational-related subfamilies. *Protein Eng.* **1996**, *9*, 1063–1065. [[CrossRef](#)]
42. König, U.; Norberg, N. New Tools for Process Control in Aluminum Industries—PLSR on XRD Raw Data. In Proceedings of the 10th International Alumina Quality Workshop, Perth, Australia, 19–23 April 2015; pp. 305–308.
43. Wold, H. Estimation of principal components and related models by iterative least squares. In *Multivariate Analysis*; Krishnaiah, P.R., Ed.; Academic Press: New York, NY, USA, 1966; pp. 391–420.
44. Filippov, L.; Farrokhpay, S.; Lyo, L.; Filipova, I. Spodumene flotation mechanism. *Minerals* **2019**, *9*, 372. [[CrossRef](#)]
45. Groat, L.A.; Chakoumakos, B.C.; Brouwer, D.H.; Hofmann, C.M.; Fyfe, C.A.; Morell, H.; Schultz, A.J. The amblygonite LiAlPO₄F-Montebasite LiAlPO₄OH solid solution: A combined powder and single-crystal neutron diffraction and solid state Li MAS, COP MAS and REDOR NMR study. *Am. Mineral.* **2003**, *88*, 195–210. [[CrossRef](#)]
46. Grosjean, C.; Miranda, P.H.; Perrin, M.; Poggi, P. Assessment of the world lithium resources and consequences of their geographic distribution on the expected development of the electric vehicle industry. *Renew. Sustain. Energy Rev.* **2012**, *166*, 1735–1744. [[CrossRef](#)]